PERGAMON

Journal of Structural Geology 21 (1999) 191–214

JOURNAL OF STRUCTURAL GEOLOGY

Deformation character and palaeo-fluid flow across a wrench fault within a Palaeozoic subduction–accretion system: Waratah Fault Zone, southeastern Australia

David R. Gray [a,*], Christoph Janssen [b], Yevgeny Vapnik [c]

[a] *VIEPS Department of Earth Sciences, Monash University, Melbourne 3168, Australia*
[b] *GeoForschungsZentrum Potsdam, Telegrafenberg A51, 14473 Potsdam, Germany*
[c] *Department of Geology, Ben-Gurion University, P.O. Box 653, Beer-Sheva 84105, Israel*

Received 26 August 1997; accepted 3 November 1998

Abstract

Mélange formation, cataclasis, meso- to micro-scale faulting, and veining reflect faulting processes within turbidite and limestone sequences juxtaposed along a steeply dipping, sinistral wrench-fault zone in the Lachlan Orogen, southeastern Australia. Fault damage occurs across a zone up to 600 m wide. Effects of faulting in the turbidites are shown by a 100–150 m wide zone of scaly mudstone-matrix mélange, mud-injection 'dykes' and veinlets, and refolding of mélange fabrics, with minor subsidiary brittle-faulting and cataclasis extending up to 500 m from the major fault plane. Veining and cataclastic zones occur in the limestone and are most pronounced up to 100 m from the main brittle fault. Fluid inclusion data from quartz and calcite veins suggest faulting took place at temperatures between 160 and 200°C, whereas folding is inferred to have taken place at temperatures above 300°C. Fluid-assisted, fault zone 'weakening' mechanisms (pressure solution/solution transfer) were active over the whole fault zone. Veining, characteristic of fluid-assisted fault zone 'strengthening' processes (i.e. rock-mass cementation), is confined to the limestone sequence. Here, calcite precipation led to fault rocks with lower porosity and permeability than in the turbidite sequence. Overprinting between different veins and fractures, and zonation in vein cement suggest cyclic deformation and fluid flow. The repeated change between brittle fracturing and veining/cementation led to a combined conduit–barrier system in the limestone sequence, whereas the mélange zone in the turbidites acted as a fluid conduit only. © 1999 Elsevier Science Ltd. All rights reserved.

1. Introduction

Internal structures of fault zones and mechanisms of faulting are useful in understanding and predicting earthquakes. In particular, the observed weakness of many continental fault zones relative to the surrounding country rocks has led to a long-standing discussion concerning the mechanical behaviour of seismogenic active faults in the Earth's crust (Chester and Logan, 1986, 1987; Sibson, 1989, 1990; Hickmann, 1990; Chester et al., 1993; Chester, 1994). Seismogenic faulting however, normally located within the upper 5–20 km of the crust, is not accessible for direct observations. Therefore, experimental rock deformation and studies of exhumed fault zones have been used to explain mechanisms of faulting and to develop models of fault evolution. Laboratory experiments have provided information about the conditions under which seismogenic faulting takes place in various minerals and rocks (e.g. Paterson, 1978; Blanpied et al., 1992; Logan et al., 1992) and led to better understanding of the transition from stable sliding to stick slip behaviour (cf. Hirth and Tullis, 1989). But in naturally deformed rocks, variables such as fluid pressure, fluid composition, lithology and grain size have affected and complicated the faulting process (e.g. Newman and Mitra, 1993). Investigations of exhumed fault zones provide direct information about variations in fault zone characteristics (fault rock composition, meso- and microstructures, fault thickness, fluid flow) and changes in the strength of faults (Cox and Etheridge, 1989; Scholz, 1989; Hadizadeh, 1994; Knipe and

* Corresponding author. E-mail: dgray@earth.monash.edu.au

0191-8141/99/$ - see front matter © 1999 Elsevier Science Ltd. All rights reserved.
PII: S0191-8141(98)00115-1

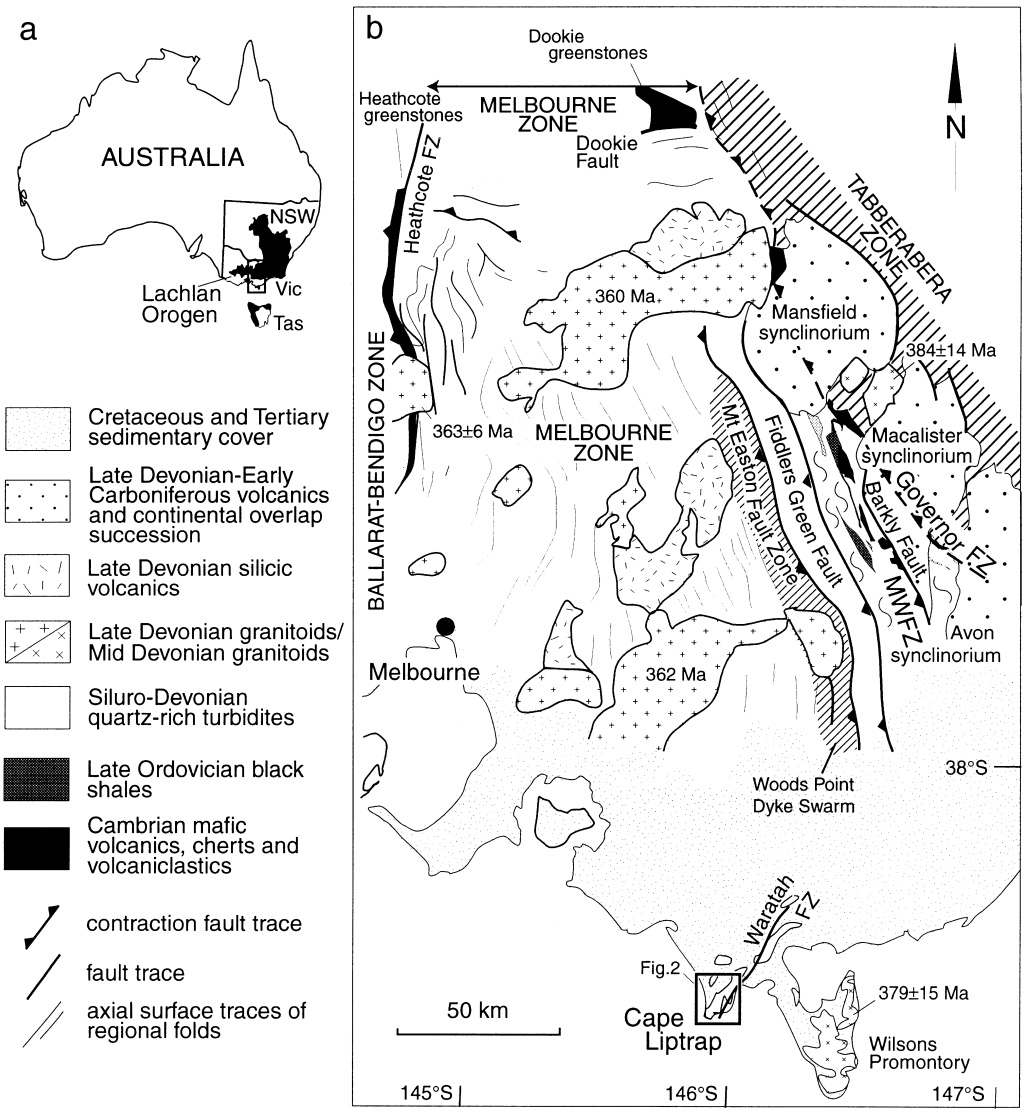

Fig. 1. Geological map of Melbourne Zone showing continental overlap successions, post tectonic granites and their volcanic carapaces and the curvilinear axial surface traces of regional folds (modified from VandenBerg, 1988, fig. 4.1). Position of Cape Liptrap and Fig. 2 is shown. MWFZ: Mount Wellington Fault Zone. Granite K/Ar age data are from Richards and Singleton (1981). The Woods Point Dyke swarm occurs in a region some 150 km long by 20 km wide, and consists of mafic/ultramafic rocks with ages ~380 Ma (Richards and Singleton, 1981). These dykes have been related to closure of the marginal sea (former Melbourne 'trough') with subsequent detachment of the oceanic slab (see Soesoo et al., 1997, fig. 3).

Lloyd, 1994; Newman and Mitra, 1993; Cox, 1995; Janssen et al., 1997).

This paper describes the character of a Palaeozoic, brittle wrench-fault in the turbidite-dominated western subprovince of the Lachlan Orogen near Cape Liptrap, southeastern Australia (Fig. 1). Deformation across the fault zone is investigated within limestone and clastic turbiditic rocks at both meso- and microscopic scales. Fluid-inclusion analyses from both quartz and calcite veins are used to estimate fold- and fault-related deformation conditions. The purpose of these investigations is, firstly to characterise the interaction of fluids with lithology, and secondly to determine their effects on deformation mechanisms and fault behaviour. Finally, the results are integrated into a model to explain the differences in fault-related deformation. The paper shows that fault zone character, local deformation mechanisms, fluid–rock behaviour, and therefore fault-zone rheology, change with lithology across the 600 m wide fault zone. The fault zone has behaved as a combined conduit–barrier system, which may typify fault behaviour and the palaeo-fluid flow of faults in the shallow levels of accretionary prisms or sediment wedges. A companion paper (Janssen et al., 1998) investigates the nature of the fluid and the alteration effects around the Waratah

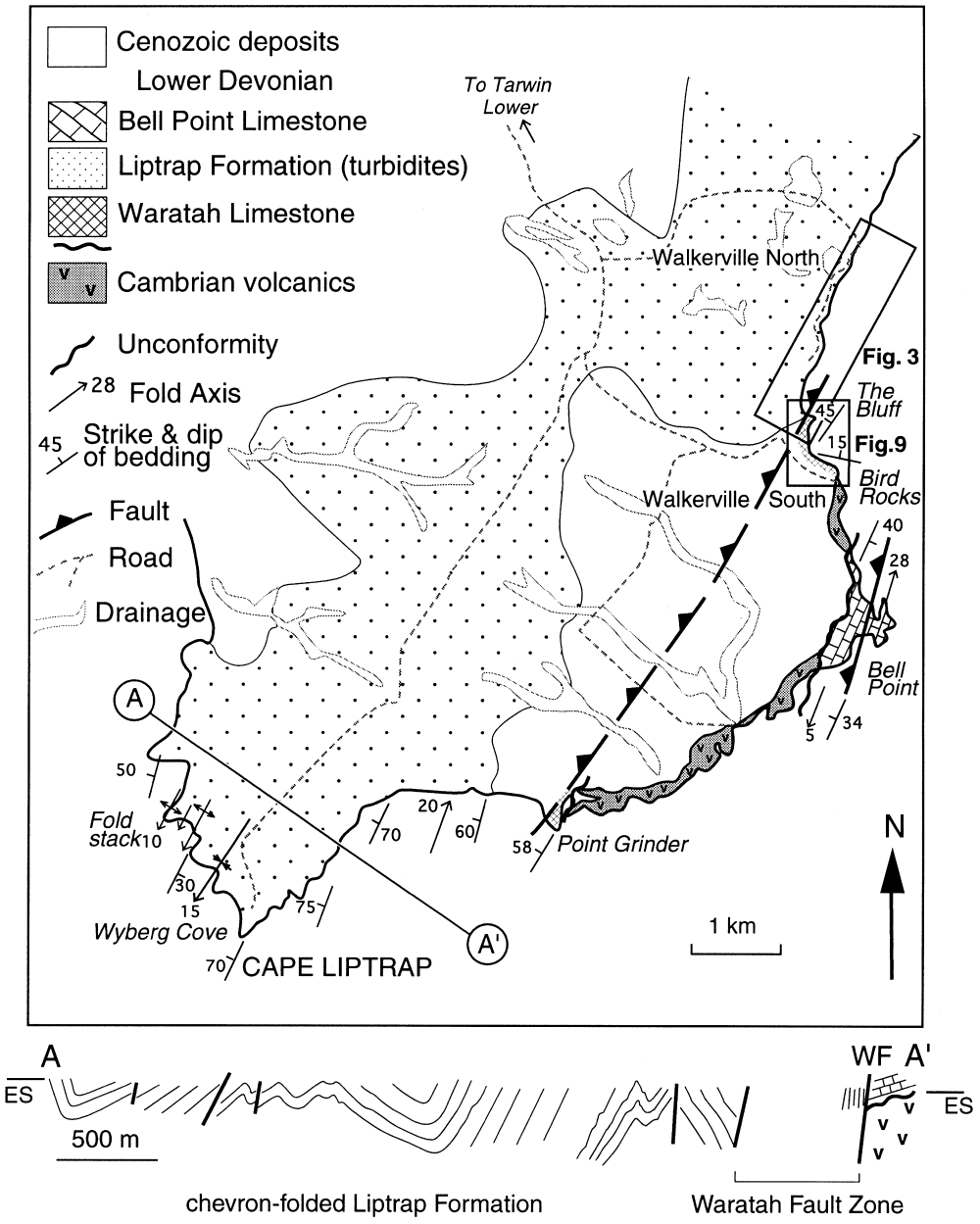

Fig. 2. Geological map of the Cape Liptrap region showing the Liptrap Formation in fault contact with Early Devonian limestone overlying a Cambrian metabasalt–chert sequence along the Waratah Fault (modified from Lindner, 1953, fig. 3; and O'Connor, 1978). Locations of Figs. 3 and 9 are shown. Structural profile A–A′ adapted from O'Connor (1978).

Fault Zone, using major and minor element geochemistry and stable isotopes of veins.

2. Geological setting of the Waratah Fault Zone

The Waratah Fault Zone is a steep, NE–SW-trending, 'brittle' fault zone which juxtaposes a weakly cleaved, chevron-folded turbidite sequence with minor (<1%) quartz veins (Early Devonian Liptrap Formation) against heavily veined and fractured limestone (Early Devonian Bell Point Limestone). It is located in the eastern part of the Melbourne Zone (Fig. 1) in the western subprovince of the mid-Palaeozoic Lachlan Orogen (Gray, 1997, fig. 4). The western subprovince consists of an east-vergent, accretionary wedge-type thrust-system (Gray and Foster, 1998). This occurs within an Early Palaeozoic turbidite sequence consisting of chevron-folded, interbedded sandstone and mudstone (Cox et al., 1991; Gray and Willman, 1991a,b; Gray et al., 1991; Gray and Foster, 1997; Gray and Foster, 1998). Slivers of 'oceanic' crust are preserved within major faults which bound three major structural zones (Gray, 1997, figs. 3 and 4). The

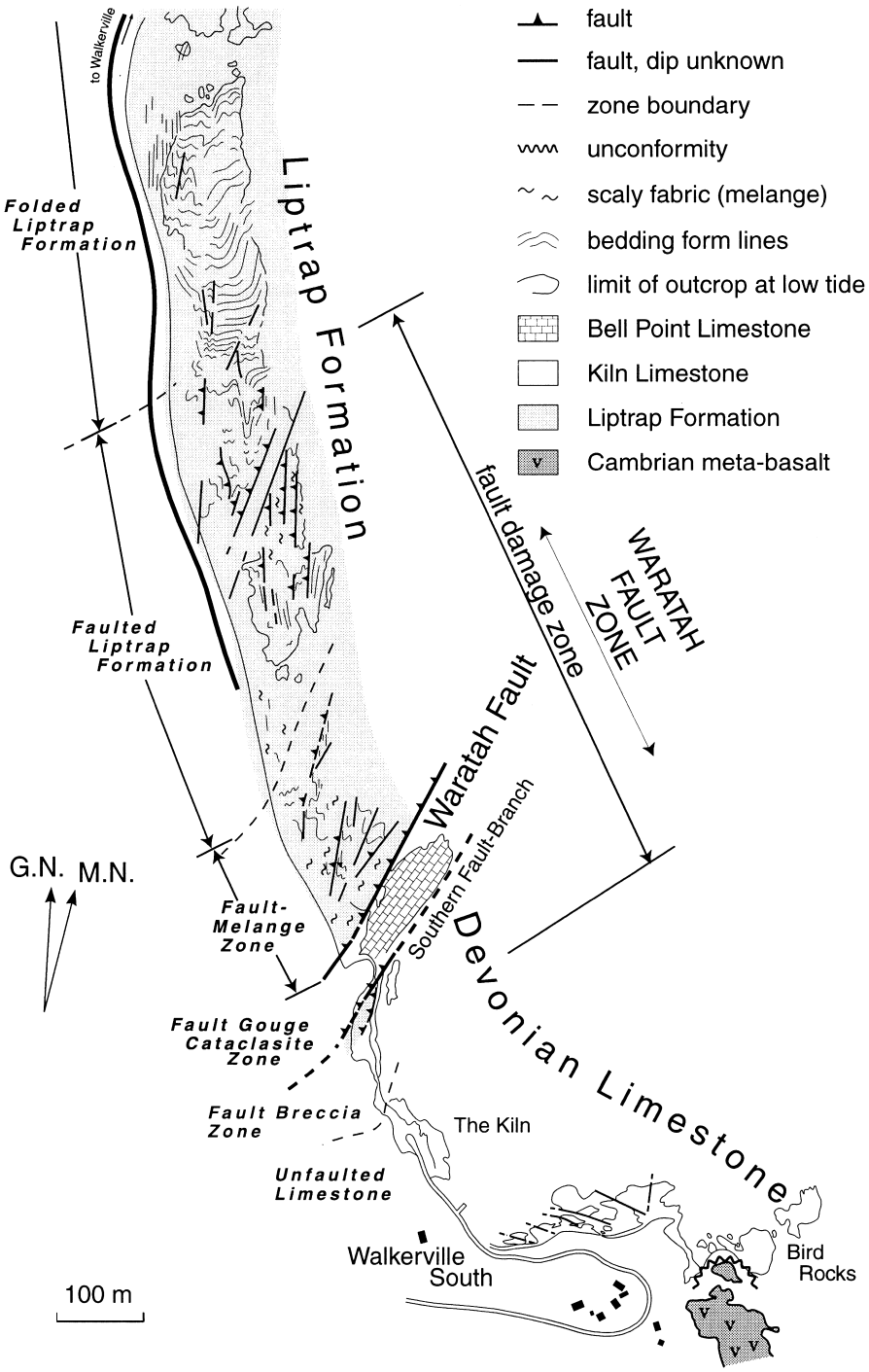

Fig. 3. Geological map of the Waratah Fault Zone on the foreshore of Waratah Bay between Walkerville North and Walkerville South. Structural zones for the Waratah Fault Zone are shown.

Waratah Fault Zone may form part of a wrench transfer-zone between east-vergent structures in the Melbourne Zone (Murphy and Gray, 1992; Gray, 1995; Gray and Mortimer, 1996) and west-vergent structures in the Mathinna Beds of northern Tasmania (Powell and Baillie, 1992; Elliott et al., 1993; Woodward et al., 1993).

The Waratah Fault Zone separates a sequence of Early Devonian quartz sandstones and mudstones (Liptrap Formation) from Early Devonian Siegenian and Emsian limestones (Bell Point Limestone, Kiln Limestone, Bird Limestone; Figs. 2 and 3) (Lindner, 1953; Talent, 1965; VandenBerg, 1975). The Liptrap Formation is close to tightly chevron-folded (Fig. 2,

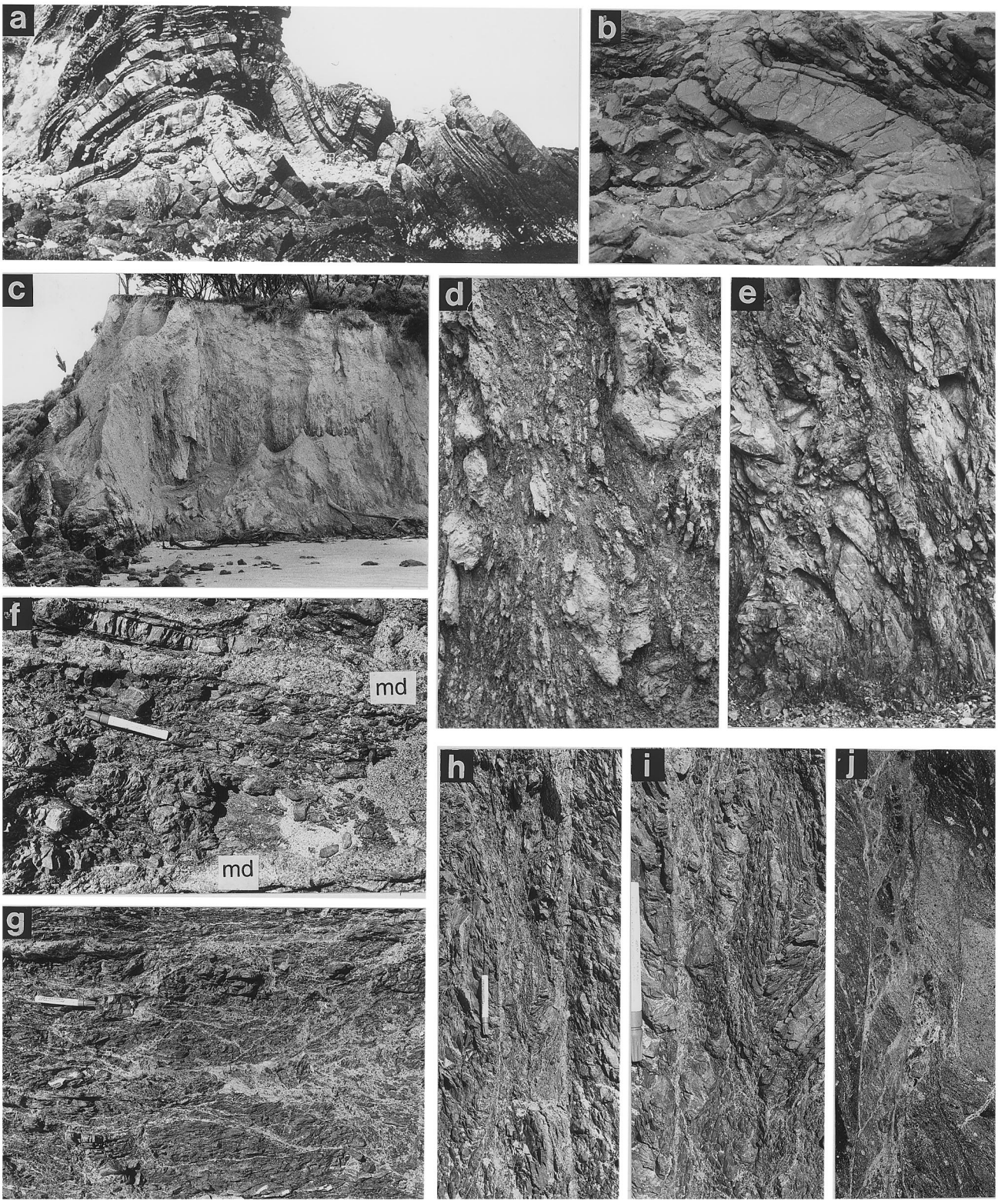

Fig. 4. Photographs of fold- and fault-related deformation structures in the Liptrap Formation. (a) Typical folds in the Liptrap Formation, Fold Stack (see Fig. 2). Base of photo approx. 20 m. (b) Slump folds in Liptrap Formation, between Point Grinder and Cape Liptrap. Base of photo is approx. 5 m. (c) Waratah Fault at the Bluff, Walkerville South. Base of photo is approx. 15 m. (d) Sandstone blocks in scaly-matrix mélange of the fault mélange zone, the Bluff. Base of photo is approx. 1 m. (e) Fractured Liptrap Formation transitional into mélange, the Bluff. Base of photo is approx. 2 m. (f) Mud injection dykes (md) intruded subparallel to the foliation in the scaly-mudstone matrix mélange, the Bluff. Pen length is 16 cm. (g) Fine anastomosing mud-injection veinlets intruded subparallel to the foliation in the scaly-mudstone matrix mélange, the Bluff. Pen length is 16 cm. (h) Mud injection zones subparallel to cataclastic zones within brecciated Liptrap Formation, the Bluff. Pen length is 16 cm. (i) Enlargement of (h) showing folded scaly mudstone fabric truncated by cataclastic zones and intruded by mud injection veins. Pen length is 16 cm. (j) Photomicrograph of anastomosing cataclastic zones in Liptrap Formation, the Bluff. Base of photo is 2 cm.

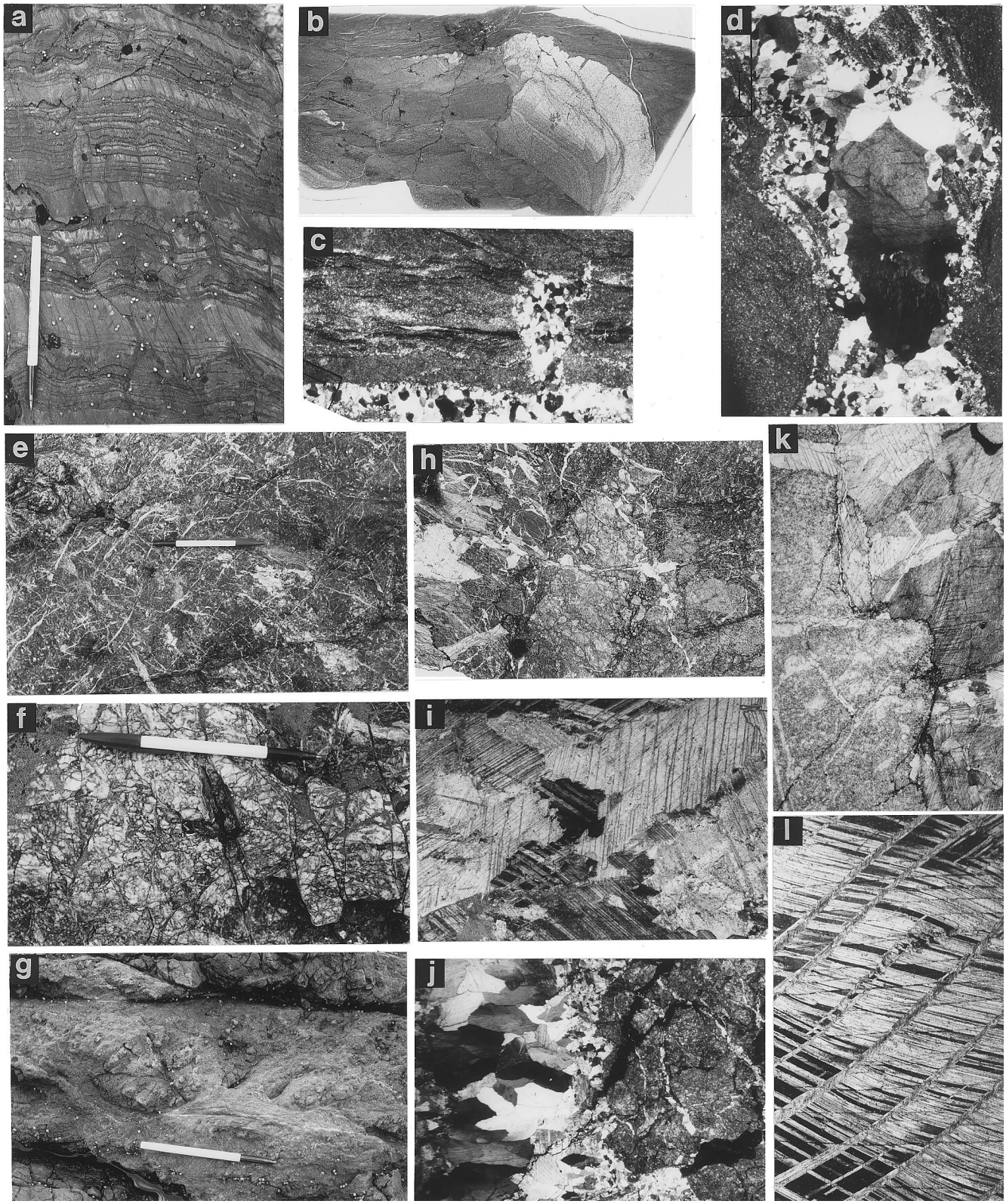

Fig. 5 (*caption opposite*)

section A–A′; Fig. 4a), but the mudstones are only weakly cleaved (Fig. 5a). The limestones are cataclastically deformed, weakly folded, and contain rare tectonic stylolites. The Early Devonian limestones rest unconformably upon Cambrian meta-basalts which comprise massive basalt, pillow lavas and intercalated umber and ochre cherts (Fig. 2). Limestone detritus within slumped horizons and fragments of greenstone within coarse sandstone units in the turbidites, suggest a local source component for the Liptrap Formation (Nas, 1988).

The Melbourne Zone contains a thick, unbroken Silurian–Lower Devonian sedimentary succession, but shows progradation in sedimentation from west to east (Garrat, 1983; VandenBerg, 1988, table 4.1; Foster et al., 1996). In the west a 9–10-km-thick basal Silurian to Pragian sequence (Darraweit Guim province) thins to approximately 2.2 km in the east (Mount Easton province) (Ramsay and VandenBerg, 1986, p. 225; VandenBerg, 1988). The Early Devonian successions are marked by shallowing in the west and turbidite deposition in the east (> 5 km). Sedimentation was terminated after deposition of a 2–4-km-thick late Early Devonian (Eifelian–Frasnian) sequence (VandenBerg and Wilkinson, 1982). Ages of 450–430 Ma for the inherited detrital mica components in the eastern Melbourne Zone (Bucher et al., 1996), suggest cannibilisation of the Cambrian–Early Ordovician quartz-rich turbidites in the zones to the west, accompanying the west to east progradation in sedimentation (Foster et al., 1996, 1998).

The single Early–Middle Devonian deformation of the Melbourne Zone is constrained by the age of the youngest Eifelian sediments (380–387 Ma) and ages of post-tectonic granites (362–376 Ma; VandenBerg, 1988; Gray, 1990; Gray and Cull, 1992). $^{40}Ar/^{39}Ar$ mica crystallisation ages from the western Lachlan Orogen indicate that deformation migrated eastwards from 450 Ma in the west to ~400–390 Ma in the east while sedimentation was ongoing in the eastern Melbourne Zone (Foster et al., 1996, 1998; Gray and Foster, 1997; Gray et al., 1997). The Liptrap Formation represents some of the last sediments deposited. Deformation is considered to have occurred soon after or during sedimentation (< 10 Ma), an argument supported by slumped zones and slump horizons in the Liptrap Formation, features not typical of other parts of the western subprovince of the Lachlan Orogen (cf. Cas and VandenBerg, 1988). Zones of slump folds up to 50 m wide in the Liptrap Formation are defined by variously oriented, highly irregular folds (Fig. 4b) often with complex fold interference and bounded by faults (Gray, unpublished data).

Subgreenschist metamorphism is characterised by white mica, chlorite and minor metamorphic muscovite assemblages in the arenites and mudstones of the Liptrap Formation (Lennox and Golding, 1989; Offler et al., 1998). The presence of intermediate *P* metamorphism within the turbidites shown by the 'b_o' cell spacing of white mica in slates (Offler et al., 1998), and intermediate–high *P* blueschist metamorphism shown by relict Na amphiboles in Cambrian mafic volcanics and Franciscan-like blocks within serpentinite and mud-matrix mélanges (see Nicholls, 1965; Spaggiari et al., 1998) support deformation in an oceanic setting, with the inferred underthrusting (e.g. Murphy and Gray, 1992; Gray, 1995) potentially related to subduction (see Gray and Foster, 1997; Soesoo et al., 1997). Geological relationships and deformation style suggest that in the Early Devonian this part of the Melbourne Zone was in the frontal part of a migrating sedimentary 'wedge' analogous to an accretionary prism within a SW Pacific-style marginal sea or small ocean basin (Foster et al., 1996; Gray and Foster, 1997; Foster and Gray, in press).

3. Fault zone character

The Waratah Fault was first recognised as a NE–SW-trending, steeply W-dipping, brittle fault (Lindner, 1953). It has a map length of about 40 km (Fig. 1b) and has been considered to be a continuation of the Mount Eastern Fault Zone (cf. VandenBerg and

Fig. 5. Photographs of fold- and fault-related deformation structures in the Liptrap Formation (a–d), the limestones (e, f, h–l) and the mafic volcanics (g). (a) Spaced cleavage in fine grained sandstone layers and weak reticulate to slaty cleavage in mudstone of the Liptrap Formation, Walkerville North. Pen length is 14 cm. (b) Weakly developed slaty cleavage in mudstone showing folded, fine grained sandstone layer, Liptrap Formation, the Bluff. Base of photo is 8 cm. (c) Dark pressure solution seams marking the slaty cleavage, cut by post-cleavage, discordant, fault-related quartz vein. Base of photo is approx. 5 cm. (d) Quartz vein in mudstone filled by coarse quartz cement, showing increasing grain size toward the vein centre. Crossed nicols. Base of photo is 3 cm. (e) Heavily veined and fractured, cataclasitic Bell Point Limestone near the Waratah Fault, the Bluff. Pen length is 14 cm. (f) Heavily veined and fractured, cataclasitic Waratah Limestone near the Waratah Fault, Point Grinder. Pen length is 14 cm. (g) North-trending cataclastic zone in the Cambrian metabasites, Bird Rocks. Pen length is 14 cm. (h) Photomicrograph of veined and fractured cataclasite, Bell Point Limestone, the Bluff. Base of photo is 5 cm; PPL. (i) Photomicrograph of calcite cement in brecciated Bell Point Limestone close to the fault contact showing lattice-controlled 'bulging' grain boundaries due to dynamic recrystallisation. Base of photo is approx. 1 mm; crossed nicols. (j) Calcite vein between clay-gouge (right) and Bell Point Limestone showing elongated blocky calcite indicative of slow opening by aseismic slip (cf. Gratier and Gamond, 1990). Base of photo is 3 cm; crossed nicols. (k) Brecciated Kiln Limestone showing stylolitic contact between twinned vein-cement and unchanged limestone matrix. Base of photo is 6 mm; crossed nicols. (l) Bent and intersecting deformation twins in calcite vein within brecciated Bell Point Limestone. Base of photo is approx. 1 mm; crossed nicols.

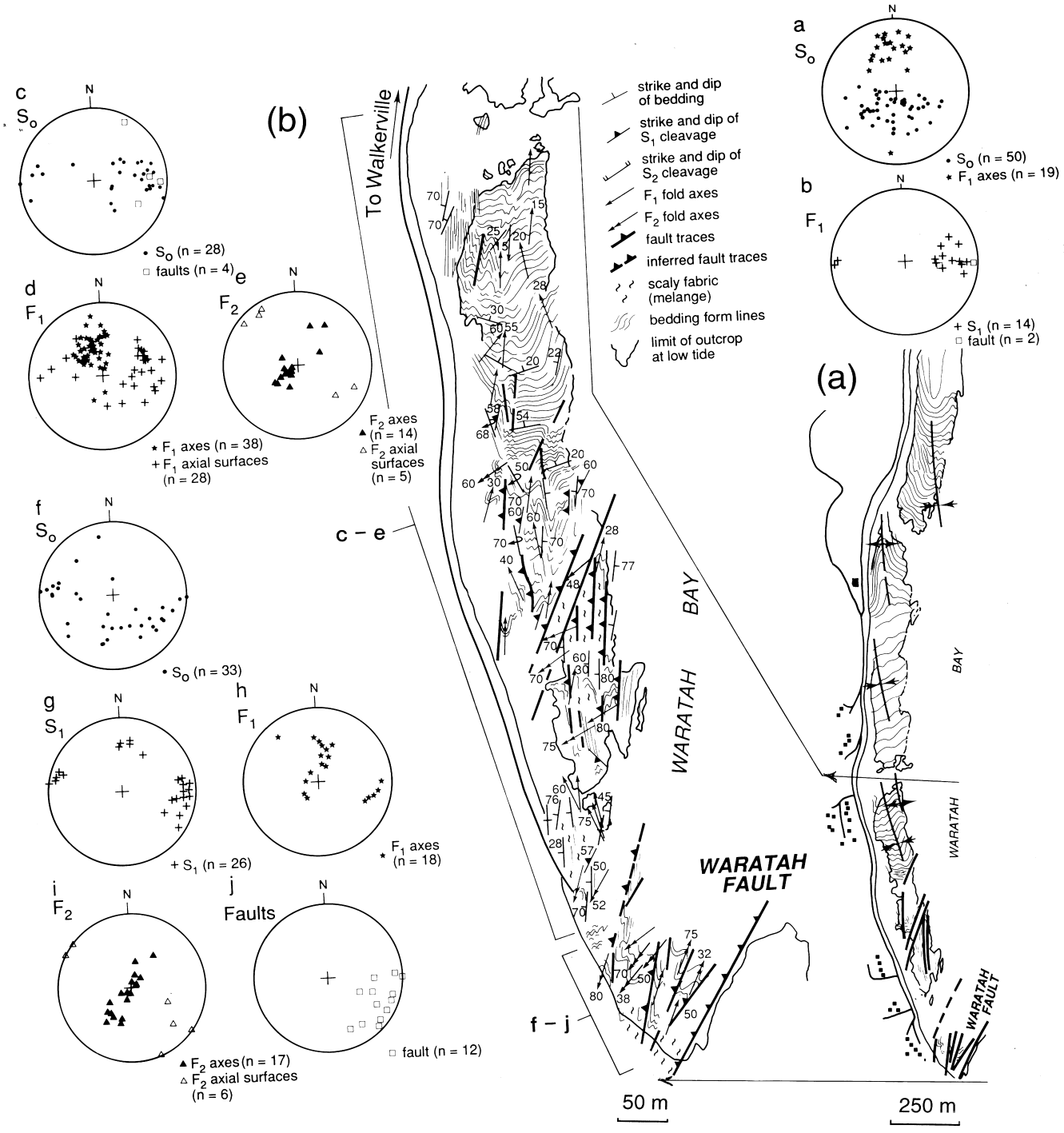

Fig. 6. Structural maps (a) and (b) of the folded and faulted Liptrap Formation north of the Waratah Fault Zone, with an enlarged form surface map (B) of the region adjacent to the Waratah Fault; see (a). Stereonets (a–j) are plots of poles to structural elements and fold axis data within the Liptrap Formation. Stereonets (a) and (b) are from 'folded' Liptrap Formation zone (see Fig. 3) away from the influence of the Waratah Fault, whereas (c), (d) and (e) are from the 'faulted' Liptrap Formation zone, and stereonets (f–j) are for structural data from the 'fault-mélange zone' (see Fig. 3).

Wilkinson, 1982; Gray, 1988). In the coastal exposures at Walkerville South (Fig. 2) the fault is a deformed region up to 600 m wide where fault-mélange/gouges, cataclasites, and fault-breccias surround and incorporate lenses and pods of less deformed rocks (Figs. 3–5). The contact between the fault-mélange zone and the Bell Point Limestone is defined as the major fault trace (Fig. 4c), and is marked by an exposed fault plane of several tens of square metres. This contact is sharp and distinct, whereas the boundary with the damaged

Liptrap Formation is gradual and only discernible by increasing numbers of fragments imbedded in a scaly mudstone-matrix (Fig. 4d and e). Subhorizontal slickensides in the footwall limestones on the major fault plane suggest late stage, sinistral strike-slip movement along the fault. The exposed fault area and rocks adjacent to the fault were divided into six sub-areas based on lithology, deformation style and intensity of deformation with respect to distance from the main fault trace (Fig. 3).

3.1. Effects of faulting within the turbidite sequence

The interbedded sandstone and mudstone sequences of the Early Devonian Liptrap Formation show varying effects of faulting, related to distance from the major fault trace of the Waratah Fault Zone (Fig. 3).

3.1.1. Folded Liptrap Formation (distances greater than 500 m from the fault trace; Fig. 3)

Away from the Waratah Fault Zone the Liptrap Formation consists of N-trending chevron-folds cut by N- and NW-trending brittle faults (Fig. 6a, stereonets a, b). The regional fold deformation is characterised by gently to moderately plunging angular chevron folds with planar limbs (Figs. 2 and 4a and Fig. 6, stereonets a, b, c) (cf. Lennox and Golding, 1989). Fold tightness, fold-hinge geometry and cleavage development varies with lithology; folded mudstone beds show angular forms and mostly close fold tightness whereas more rounded, open folds dominate in sandstone facies. Mudstones show a weak, spaced to sometimes irregular, reticulate cleavage (Fig. 5a) and sandstones a heterogeneously developed, spaced cleavage (Fig. 5b). Minor quartz veins ($<1\%$) are present.

3.1.2. Faulted Liptrap Formation (distances between 500 and 150 m from the fault trace; Fig. 3)

As the fault zone is approached the folded Liptrap Formation becomes broken up by a developing fault-mélange system dominated by N-trending faults cut by NE-trending fault zones (Fig. 6b, stereonets). Plunges of early folds tend to steepen somewhat (Fig. 6, compare stereonets a, d, h) and they are refolded by smaller, NE-trending folds (F_2) (Fig. 6, stereonets e, i). The later folds (F_2) have steep dipping to subvertical axial surfaces, and moderate to steep either NNE- or SSW-plunges (Fig. 6, stereonet e). These folds show no associated axial surface foliation. The fault-related deformation is characterised by small faults, ranging from $\sim$10 cm to greater than 10 m in length, which cut through the folded mud- and sandstone layers dismembering F_1 and F_2 folds. Both these faults and the F_2-fold axial surface strike roughly parallel to the major fault trace and become more prominent toward the fault mélange zone (Fig. 6, stereonets c, d, e). Only a few small veins were observed (in the position of Riedel shears) suggesting that veining activities during faulting are negligible (see Section 8). The transition from the damaged Liptrap Formation to the fault mélange zone is gradual.

3.1.3. Fault-mélange zone (distances less than 150 m from the fault trace; Fig. 3)

Adjacent to the major fault trace the Liptrap Formation has been changed to a tectonic 'mélange' (Fig. 4c and d) with a pronounced scaly fabric oriented subparallel to the NE-trending dominant fault set (Fig. 6, stereonet j). The mélange contains polydeformed blocks of folded and cleaved turbidite (Figs. 7 and 8). F_1 folds generally N-plunging (Figs. 4f and 6, stereonet f), become re-oriented and refolded by steeply NE- or SW-plunging, NE-trending F_2 folds (Fig. 6, stereonet i). Blocks of folded and cleaved Liptrap Formation up to 20–30 m in width and 50–100 m in length are surrounded by scaly mudstone-matrix mélange in the main fault zone (Fig. 7). These contain both F_1 and F_2 fold structures. F_2 folds fold the early-formed weak S_1 cleavage, but do not develop any axial surface foliation (Fig. 8, insets b, c). Close to the fault trace, the mélange zone is characterised by an overall increase in development of a scaly fabric (Fig. 8) with relict isoclinal fold-noses in segmented sandstone layers (Fig. 8, inset a). Fragments and fractures within the mélange (Fig. 4e) display a strong preferred orientation parallel to the fault (Fig. 6, steronet c). Mud injection zones as dykes (Fig. 4f) and veinlets (Fig. 4g) form an anastomosing system within distributed microfractures and mesofractures. The larger (up to 4 cm width) dyke-like zones contain sub-rounded to subangular fragments of sandstone and chert up to 1.5 cm in diameter in a grey mudstone matrix.

Fault-related veins in the fault-mélange zone are extremely rare, and were formed oblique to the NNE-oriented scaly fabric of the mélange matrix. The veins vary between 2 mm and 2 cm in width and are filled by coarse quartz-cement, displaying an increase in grain size away from the vein surfaces (Fig. 5d). In some veins the remaining pore spaces between the quartz grains are filled by calcite.

3.2. Effects of faulting within the limestone

Fault-related brittle deformation has resulted in the formation of fault-gouges and cataclasites (fault-gouge cataclasite zone, Fig. 3), fault breccias (fault-breccia zone, Fig. 3), and slightly deformed host rocks (unfaulted limestone zone, Fig. 3). The intensity of fracturing and cataclasis drops off markedly at approximately 150 m from the main fault trace, where limestones are only weakly deformed due to broad warping. This folding in the limestones is characterised

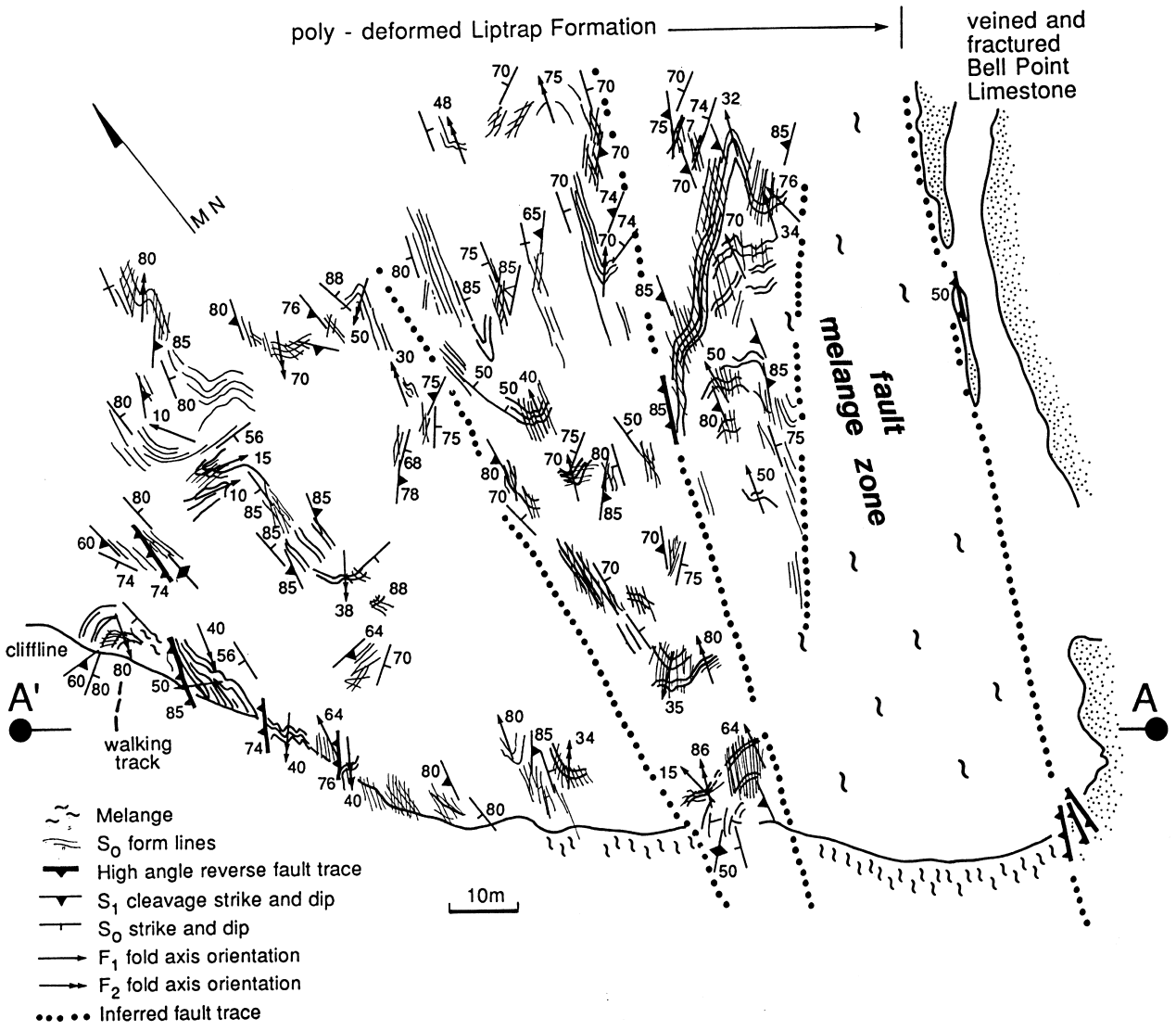

Fig. 7. Structural form surface map of the fault-mélange zone developed within Liptrap Formation turbidites. Scaly-matrix mélange surrounds relict blocks of Liptrap Formation showing two generations of folds. A–A′ is section line for profile of Fig. 8.

by open, gently plunging folds (Fig. 9, stereonet a), with rare NW-trending subvertical stylolites (Fig. 9, stereonet b) and minor veins (Fig. 9, stereonet d) within parts of the Kiln Limestone member.

3.2.1. Fault gouge–cataclasite zone (Fig. 3)

Pervasively brecciated Bell Point Limestones define a zone of gouge material (Fig. 5e) between the major fault trace of the Waratah Fault Zone and a southern fault-branch (Fig. 3). The gouge zone contains subsidiary faults and associated intense macro-fracturing. The subsidiary faults either form conjugate fault sets or a series of fracture zones striking subparallel to the major fault plane (Fig. 10, stereonet a). The transition between brecciated limestone and the fault-gouge zone is gradual and reveals a cataclastic progression toward the fault-gouge (breccia, cataclasites and ultracataclasite) over a distance of about 1 m. The cataclastic zone near the fault-gouge possesses a centimetre-scale foliation, or spaced disjunctive cleavage, defined by preferred orientation of slivers (cleavage domains) and curved fractures (cleavage planes).

The fault-gouge zone of the southern fault branch forms the contact with the less deformed Kiln Limestones (Fig. 9). The gouge zone consists of an 8 m wide, dark-brown, fractured and extremely fine-grained, scaly-matrix mudstone. Fissility within the 'mudstone' matrix is oriented parallel to the main fault plane. Although mesoscopically homogeneous in appearance, thin sections reveal that the fault-gouge zone consists of a small marginal limestone gouge (< 10 cm) and a central clay-gouge zone (7–8 m). The limestone gouge is composed of a brown fine grained (< 10 nm) calcite-bearing clay matrix containing lenti-

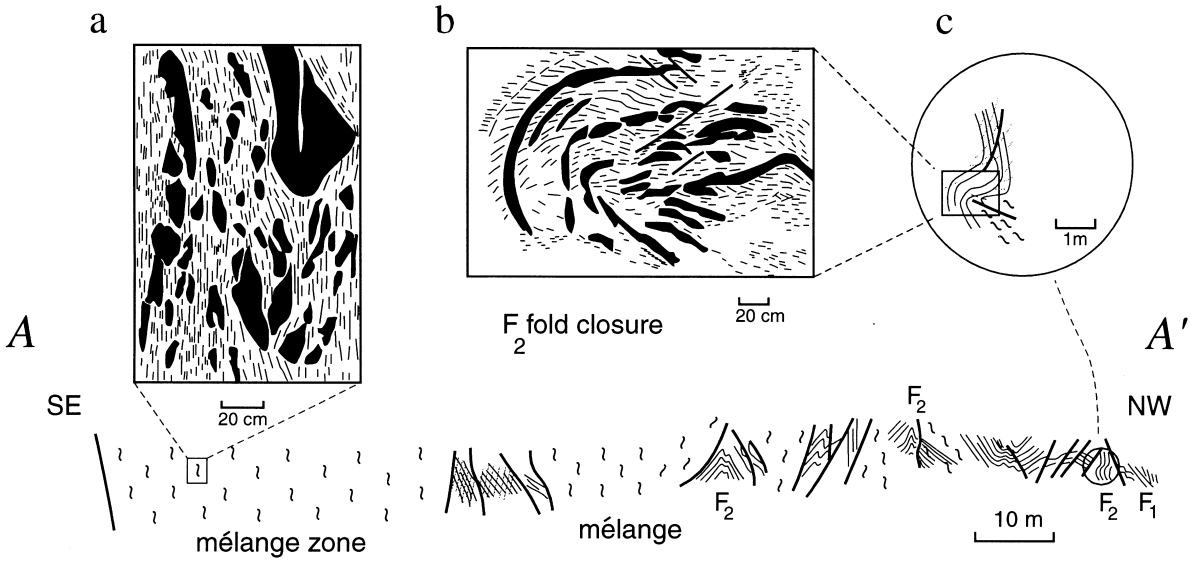

Fig. 8. Structural profile across the fault-mélange zone in the poly-deformed part of the Liptrap Formation. Accompanying structural sketches include: (a) rootless isoclinal fold closure in disrupted and boudinaged psammitic layers within scaly-mudstone matrix of the mélange. (b) and (c) Detail of F_2 fold closure in relict block surrounded by mélange. Note the folding of the early formed S_1 cleavage and the lack of cleavage developed axial surface to the F_2 fold.

cular-shaped limestone fragments. Fractures are mostly healed by calcite cement. The central clay-gouge zone contains claymatrix only. Overall, the fault-gouge zone is texturally similar to the fault-mélange zone. Considering the thickness and appearance of the fault-gouge zone, it is likely that the gouge material was derived from the former Liptrap Formation (see also Janssen et al., 1998).

3.2.2. Fault breccia zone (Fig. 3)

The fault-breccia zone consists of heterogeneously deformed, heavily brecciated and veined Kiln Limestones (Fig. 5f). The fault breccias are completely healed by calcite cement and only a few thicker veins can be distinguished. Fracture sets are NW-trending, E–W-trending, or NE-trending parallel to the strike of the main fault (Fig. 10, stereonet b). At the contact with the fault-gouge zone of the southern fault branch, the Kiln Limestone appears undeformed.

3.2.3. Unfaulted limestone (Fig. 3)

Decreasing deformation intensity away from the main fault is marked by a transition from fault-breccia to faulted limestones to unfaulted limestones. Weakly deformed Kiln Limestone (Fig. 9) contains subsidiary faults and fracture zones which show more scatter than those in the fault-breccia zone (Fig. 10, compare stereonets d, h with stereonets b, f).

4. Deformation processes within the fault zone

Microscopic observations in the turbidites of the folded Liptrap Formation indicate that brittle fracturing is more important in sandstones, whereas pressure solution is dominant in mudstones (cf. Lennox and Golding, 1989). Micro-fractures, pressure solution seams and veins overprint the fold-related cleavage fabric as fault-related deformation with development of mélange increases towards the fault-mélange zone (Fig. 7b). In some cases however, fold- and fault-related structures show mutually cross-cutting relationships, suggesting perhaps a transition from fold- to fault deformation. Cleavage in scaly-mudstone within the fault-mélange zone (Fig. 3) is more intense, as shown by closer spacing of cleavage lamellae and lower bedding–cleavage angles. It is defined by dark seams of insoluble material (pressure solution relicts) that impart a striping through the rocks and a strong mica preferred orientation (Fig. 5c). A common observation in mélange/gouge zones of exhumed faults both here (Fig. 4h–j) and elsewhere is that fracturing, frictional sliding and rotation of fragments were the dominant strain-accommodating mechanisms during faulting (Chester and Logan, 1986; Chester et al., 1993; Hadizadeh, 1994). In contrast to many of these faults however, fluid-assisted faulting processes in the fault-mélange zone of the Waratah Fault Zone are restricted to processes aiding fault zone weakening (e.g. pressure solution and scaly fabric development), whereas fluid-assisted healing processes (e.g. veining

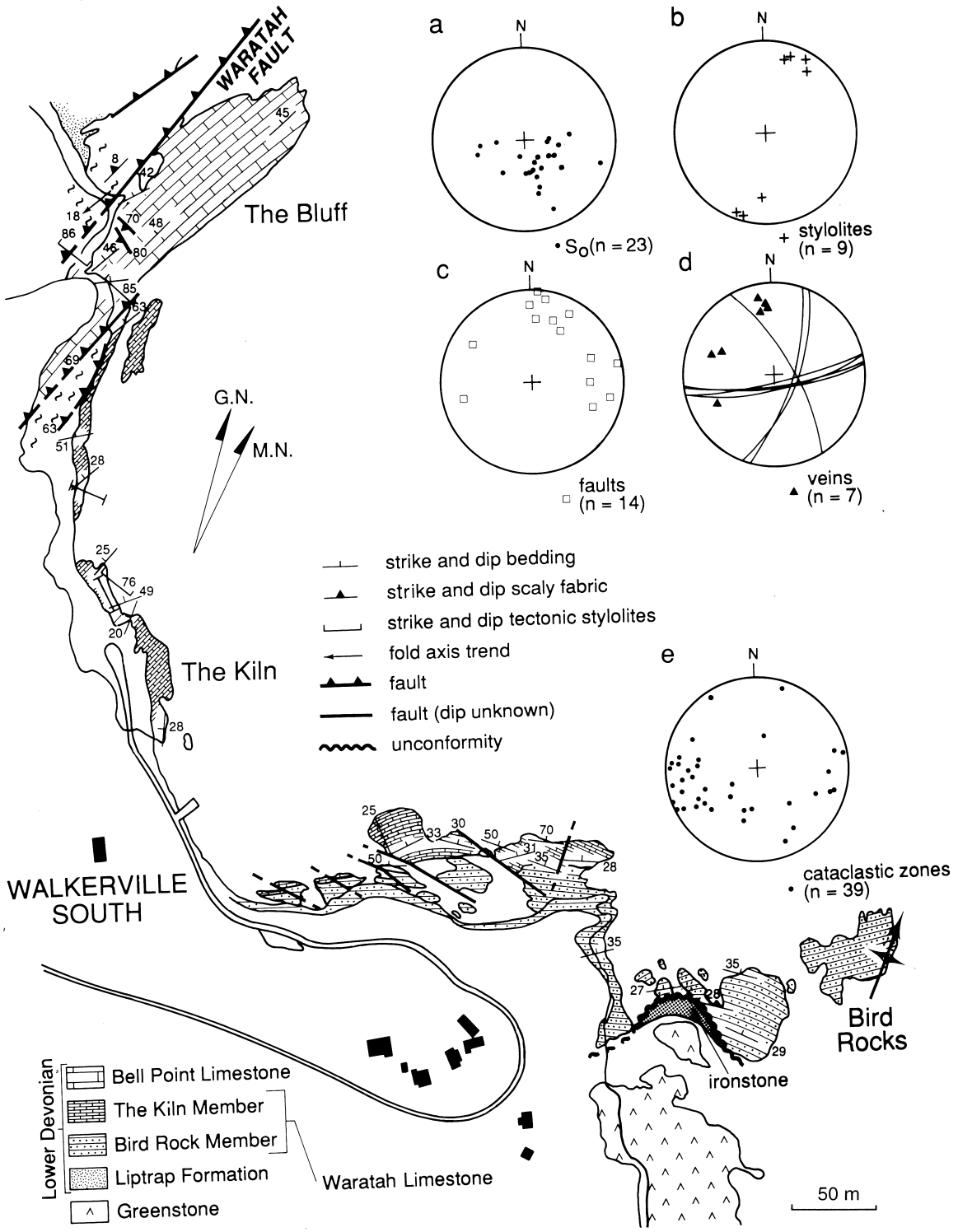

Fig. 9. Geological map with structural data of the limestone sequence on the south side of the Waratah Fault. The Bell Point Limestone occurs as a heavily fractured and brecciated homoclinally NW-dipping unit between the main fault trace and the southern branch fault (see Fig. 3). Stereonets show poles to (a) bedding, (b) tectonic stylolites, (c) faults and (d) calcite veins in limestones. Stereonet (e) shows poles to cataclastic zones within the Cambrian metabasalts exposed just south of Bird Rocks.

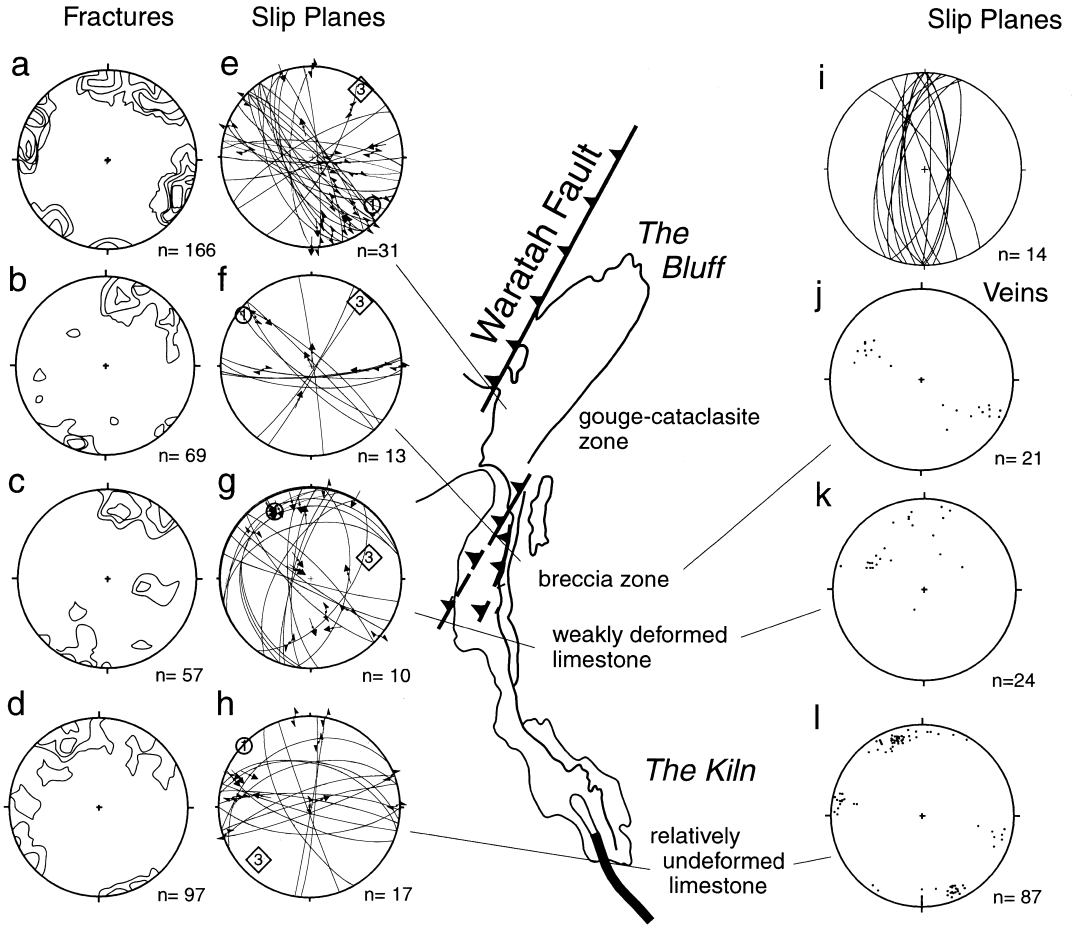

Fig. 10. Orientation data for brittle deformation elements within the Bell Point and Kiln Limestones including fractures, faults and cataclasite zones as contoured pole distributions of poles to all fractures on stereonets (a–d), fault planes and fault slip data (e–i) (lines indicate the orientation of the average main fault traces; dots indicate the striation directions measured on the fault traces; the arrows represent the sense of slip of the hanging wall and the numbers 1 and 3 depict the shortening and extension, respectively); and calcite veins as poles to veins on stereonets (j–l). Data shown on (a) and (e) are from the gouge-cataclasite zone; (b), (f) and (j) are from the breccia zone; (c), (g) and (k) are from weakly deformed Kiln Limestone; and (d), (h) and (l) are from relatively undeformed Kiln Limestone; (i) represents great circle traces of slip planes at a distance of 3–5 km from the main fault trace. Contoured pole distributions are based on a contour interval of 2.0%/1% area.

and rock-mass cementation), leading to fault strengthening, are limited.

Bell Point Limestones adjacent to the main fault trace (fault-gouge cataclasite zone, Fig. 3) are heavily brecciated, fractured and veined (Fig. 5e, f and h) indicating that brittle deformation and fluid-assisted healing processes (veining) were active during faulting. Pressure solution (Fig. 5k), fracturing (Fig. 5e and f) and twinning (Fig. 5i and l), the dominant deformation mechanisms, become more intense toward the fault-gouge zone (Fig. 11h–l). However, the biomicritic matrix remains unchanged (Fig. 5k). Many sutured grain contacts were formed by pressure solution (Fig. 5k), although some dynamic recrystallisation has occurred, as shown by lattice-controlled interpenetrating grain boundaries (Fig. 5i). Further away from the main fault trace (fault-breccia zone, Fig. 3), the brecciated Kiln Limestones reveal the same intensity of microfracturing, pressure solution and twinning, and similar cathodoluminescence signatures of calcite cements, to those in the brecciated Bell Point Limestones.

5. Fault kinematics

5.1. Mélange zone in turbidites

A change in orientation of early structures (F_1 folds) into the fault zone, as well as geometric relationships of fault-zone related F_2 meso-folds, are important kinematic indicators of faulting and fault-related strain in the turbidites (Fig. 11). Sedimentary layering is clearly truncated by the Waratah Fault

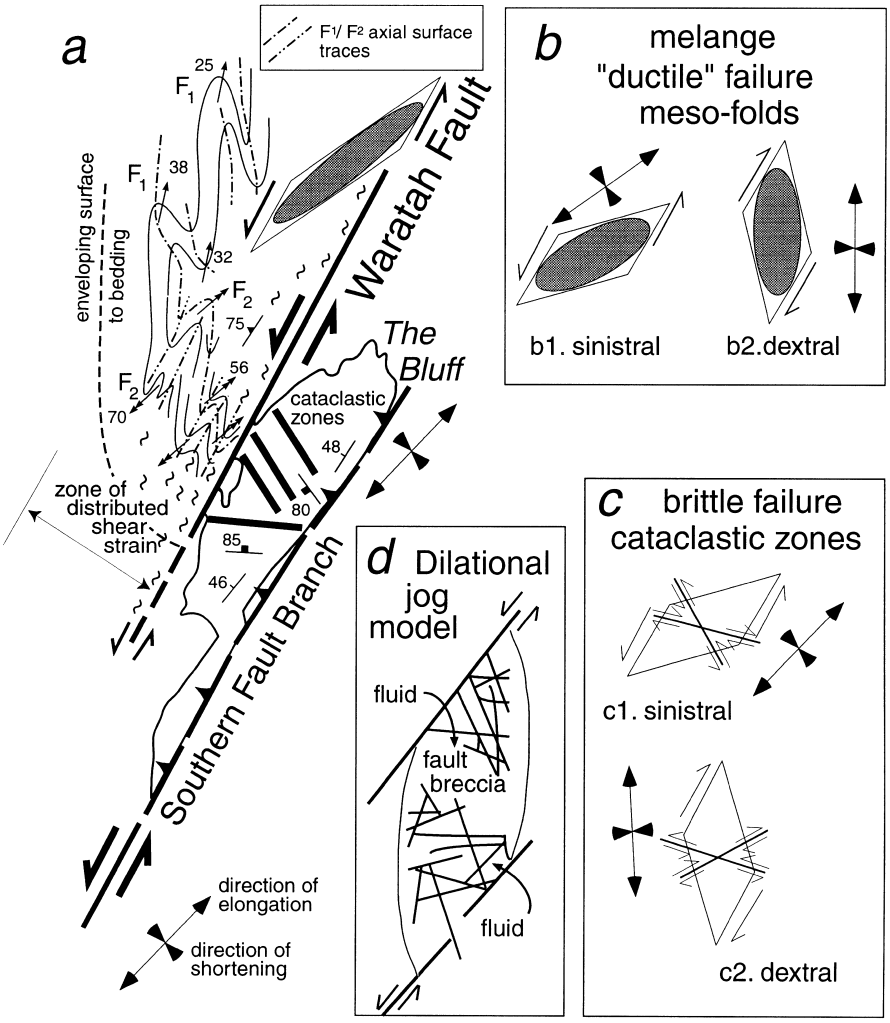

Fig. 11. Kinematic interpretation for the Waratah Fault Zone based on structural relationships and elements within the fault-mélange zone (Liptrap Formation) and the cataclasite-gouge and breccia zones (Bell Point Limestone). (a) Schematic map illustrating key relationships within the fault-mélange zone (F_2 folds and mélange, and change in orientation of the S_0 enveloping surface into the fault) and limestone (cataclastic zones). (b) Models for sinistral and dextral shear sense within NE-trending fault-mélange zone; sinistral shear produces NW-trending F_2 folds (the observed orientation), whereas dextral shear would produce N-trending folds. (c) Models for sinistral and dextral shear sense to produce conjugate fracture systems in the limestone; failure in sinistral shear produces fractures sets and slip senses which match the observed relationships (see Fig. 10). (d) Intense brecciation and cataclasis within the Bell Point Limestone may be due to implosion within a jog-segment between the main fault trace and the southern fault branch.

Zone and the enveloping surface to bedding shows a general swing from a N–S orientation to a NW–SE orientation approaching the fault, suggesting a component of sinistral wrenching (see Fig. 11a). Low angle obliquity of F_2 meso-fold axial surfaces to the fault zone boundaries, as well as the moderate to steep F_2 fold axis plunges in the mélange zone are also features typical of wrench zones (see Gray and Foster, 1998, figs. 15 and 16). The NE–SW axial surface orientation of the F_2 folds supports sinistral wrenching (Fig. 11b1). Dextral shearing within the mélange zone would produce folds with NNE–SSW-trending axial surfaces (Fig. 11b2).

5.2. Brecciated limestones

Intense development of cataclasites involving frictional slip along variously oriented fracture surfaces in the limestone provide kinematic information on fault movement within the limestone on the south side of the fault. Direction and sense of slip, indicated by striations and secondary fractures, were used to determine the orientations of the principal strain axes (see Reches, 1978, 1983; Alimendinger, 1989; Michel, 1994; Michel et al., 1995). Because of the faulting history and the relatively thick fault gouge and cataclasite zone, the striations most probably record only the last

movement on the fault and do not represent the overall finite slip direction (Chester and Logan, 1987; Marrett and Alimendinger, 1990).

Fault-slip data were obtained in the Bell Point and Kiln Limestone members (Fig. 10) and in two localities outside the area of detailed investigation. Adjacent to the main fault trace (fault-gouge cataclasite zone, Fig. 10), fault planes up to several square metres in area with subhorizontal striations cut through the brecciated limestones. Two sets of faults dominate the fault patterns; one set with some scattering in orientation comprises NW–SE to NNE–SSW sinistral fault planes and is more abundant than the other set which is composed of E–W to ENE–WSW trending faults (Fig. 10, stereonet e). Most fault planes dip at 70° (or greater). The composite fault plane solution in stereonet e (Fig. 10) shows pure wrench faulting with a shortening axis orientation of 14°/128° (as plunge/plunge direction), and an extension axis orientation of 7°/036°. The 95% confidence limit for the shortening direction is 7°.

Away from the main fault trace, within the breccia zone, faults are fewer and more heterogeneously developed (Fig. 10, stereonets f). Fault plane solutions reveal both strike-slip and reverse fault behaviour. The cumulative shortening and stretching axes are oriented 4°/306° and 17°/227°, respectively. Faults in weakly deformed limestone (Fig. 10, stereonet g) are rare, and fault slip data are therefore fewer. The composite strain axes once again indicate subhorizontal NW–SE shortening (18°/331°) and NE–SW extension (32°/071°), but the 95% confidence limit for the derived shortening axis has a spread of 19°. These match the derived strain axes from the breccia zone (compare with Fig. 10, stereonet f).

Faults in relatively undeformed limestone (Fig. 10, stereonet h) show more variable orientation than in the other subareas, but the derived composite strain axes also indicate subhorizontal NW–SE shortening (0°/312°; 95% confidence limit is 10°) and NE–SW extension (17°/227°). Faults out of the investigated area, but still adjacent to the main fault zone, have the same orientation as those within the selected sub-areas, and the derived strain axes do not change significantly when comparing shortening and extension axes adjacent to the fault with data from within the fault zone. At distances of 3–5 km from the main fault, changes in minor fault orientation and consequently in the direction of principal strain axes were observed (Fig. 10, stereonet i).

The relatively constant orientation of principal strain axes both along and adjacent to the major fault trace suggest that the whole fault zone is kinematically coherent. Orientations and movement sense of the cataclastic zones (Fig. 10) match those for sinistral shear (Fig. 11 c1), rather than dextral shear (Fig. 11 c2). For sinistral shear the maximum principal elongation direction is subparallel to the fault zone, with the shortening axis at a high angle to the zone. Angular relationships of the cataclastic zones relative to the main fault plane (Fig. 11 c1) suggest that the maximum principal compressive stress (σ_1) would have been at high angles to the fault zone (assuming that σ_1 intersects the acute bisectrix of conjugate fractures). This would indicate that the Waratah Fault Zone was weak relative to the surrounding rocks, like the present day San Andreas fault (see Rice, 1992).

6. Fluid interaction in the faulting process

Evidence of, and information about, fluid involvement in the faulting process is provided by the nature and intensity of veining, cathodoluminescence of vein cements and fault-rock matrix, and fluid inclusion data from veins both within and adjacent to the fault zone.

6.1. Veins and vein cement

Veining is largely restricted to the fault-breccia zone in the limestones on the south side of the fault (fault-breccia zone, Fig. 3). The origin and significance of these veins for fault-related deformation processes have been extensively discussed in Janssen et al. (1998). The authors distinguished between irregularly oriented vein arrays (Fig. 5e) showing transitions into cemented fault breccia zones (Fig. 5f) and thicker veins (> 10 cm) which strike parallel to the major fault trace (Fig. 10, stereonet j). Normally, in the irregularly oriented arrays, the veins are filled by drusy mosaic cement with skalenoedric crystals on the vein surfaces and blocky calcite in the centre. Intersection of twins and bent twins in vein calcites (Fig. 5l) suggests temperatures between 150 and 250°C (Burkhard, 1993). Near the main fault trace, fractures are healed by younger calcites with elongated to fibrous habit (Fig. 5j), indicating slow opening by aseismic slip (Fig. 8i; Gratier and Gamond, 1990). In these crystals, solid inclusions are parallel to the host rock interface and the crystal habits suggest episodic cracking and sealing, typical of the crack–seal mechanism (Ramsay, 1980) generally considered to be an indicator of elevated pore fluid pressure (see Section 8). The crystals are rarely twinned indicating that healing processes outlasted brittle faulting. Cross-cutting sets of veins and pressure solution seams suggest repeated episodes of fracturing and healing.

Under cathodoluminescence (CL), the original Bell Point Limestone either did not luminesce (diagenetic cements), or has only very weak CL colours (biomicritic matrix), whereas vein-cement and fault-rock matrix from samples adjacent to the main fault trace reveal

different colours and degrees of brightness suggesting that fluids with different proportions of Mn (activator of luminescence) and Fe (inhibitor) have infiltrated the fractures and altered the composition of rocks along the main fault plane. Further, several vein cement generations that are invisible in ordinary light, could be detected. An older cement generation luminesces dark orange whereas the luminescence colours of some younger veins vary from bright orange to yellow (Fig. 12a and b). Pressure solution seams with insoluble material luminesce bright yellow. The different cathodoluminescence signatures of vein cements and fine-grained matrix may suggest repeated infiltration of fluids with different trace element compositions.

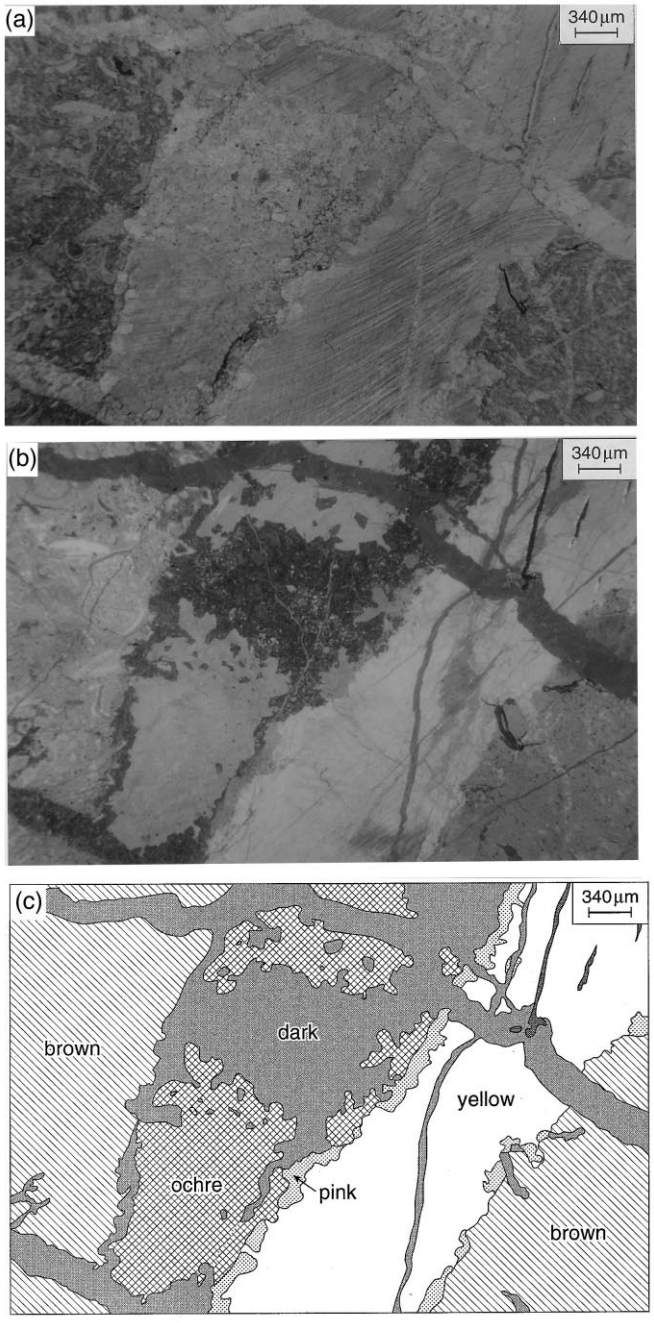

Fig. 12. Photomicrographs of deformation structures in Kiln Limestone fault breccia. (a) PPL showing two generations of calcite veins. (b) Same under cathodoluminesence (CL), and (c) sketch of the CL-photomicrograph in (b).

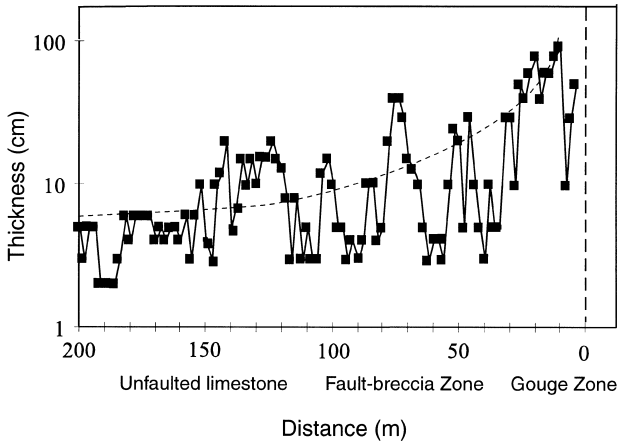

Fig. 13. Graph of vein thickness (cm) plotted against distance from the fault-gouge zone next to the main Waratah Fault trace (see Fig. 3). Note veins become bigger and thicker towards the Waratah Fault. Background veins at a distance greater than 15 m from the gouge zone have a thickness less than 1 cm.

The thicker, more isolated veins which strike roughly parallel to the main fault traces, also occur in the cataclasite and fault breccia zones (Fig. 10). Thin sections reveal that this group of veins is mostly composed of large blocky calcite cement with uniform red to orange CL-colours, whereas the host rock samples either do not luminesce or show very weak CL-colours. The boundary between host-rock veins is formed by pressure solution seams which luminesce bright orange, reflecting post-deformation alteration processes.

Away from the fault (unfaulted limestone zone, Fig. 3), calcite veins define a conjugate set, but the WNW–ESE trending veins are more abundant than NNE–SSW trending ones (Fig. 10, stereonets k, l). Microfractures and pressure solution features are less common in thin sections of these calcite veins than in vein arrays and the thicker veins. The veins are filled by two generations of mosaic calcite cement with CL-colours similar to those of unaltered host rock, suggesting that vein calcites have been locally derived. The thickness of veins changes locally, but at a larger scale these local variations are superimposed on an overall progressive increase in vein thickness toward the fault-gouge cataclasite zone (Fig. 13).

6.2. Significance of fluid inclusion data

Fluid inclusions in quartz and calcite veins (see Appendix A) show low salinities suggesting that they were trapped from the same fluid. Such low-salinity brines are typical for water of meteoric origin. Coexistence of methane and brine inclusions along the same inclusion planes, or in separate inclusion planes with the same direction and angle of dip, suggest that aqueous and gaseous fluids were trapped contemporaneously. The homogenization temperatures of aqueous inclusions in quartz (Fig. 14b) show a bimodal distribution with main temperature intervals from 200 to 250°C and from 100 to 160°C. The high temperature interval is characteristic for aqueous inclusions coexisting with methane inclusions, whereas the lower temperature interval lies in the range of the homogenisation temperatures for the aqueous inclusions in calcite (Fig. 14a). This correspondence, and the bimodal character of homogenisation temperatures in quartz, suggest that the higher temperature range may reflect folding conditions where folds formed at a deeper structural level, predating the faulting. The lower interval may characterise homogenisation temperatures during faulting at shallower structural levels.

The P–T conditions for folding and faulting, determined using intersecting isochores after Alderton and Bevins (1996, fig. 13) suggest conditions of inclusion trapping and hence the possible conditions during folding are: $T = 270$–400°C, $P = 150$–250 MPa (Fig. 14d). The data from aqueous inclusions in calcite and the low temperature inclusions in quartz probably reflect the temperature of inclusions which were trapped during the faulting event; i.e. temperatures higher than 100–160°C. In connection with microstructural investi-

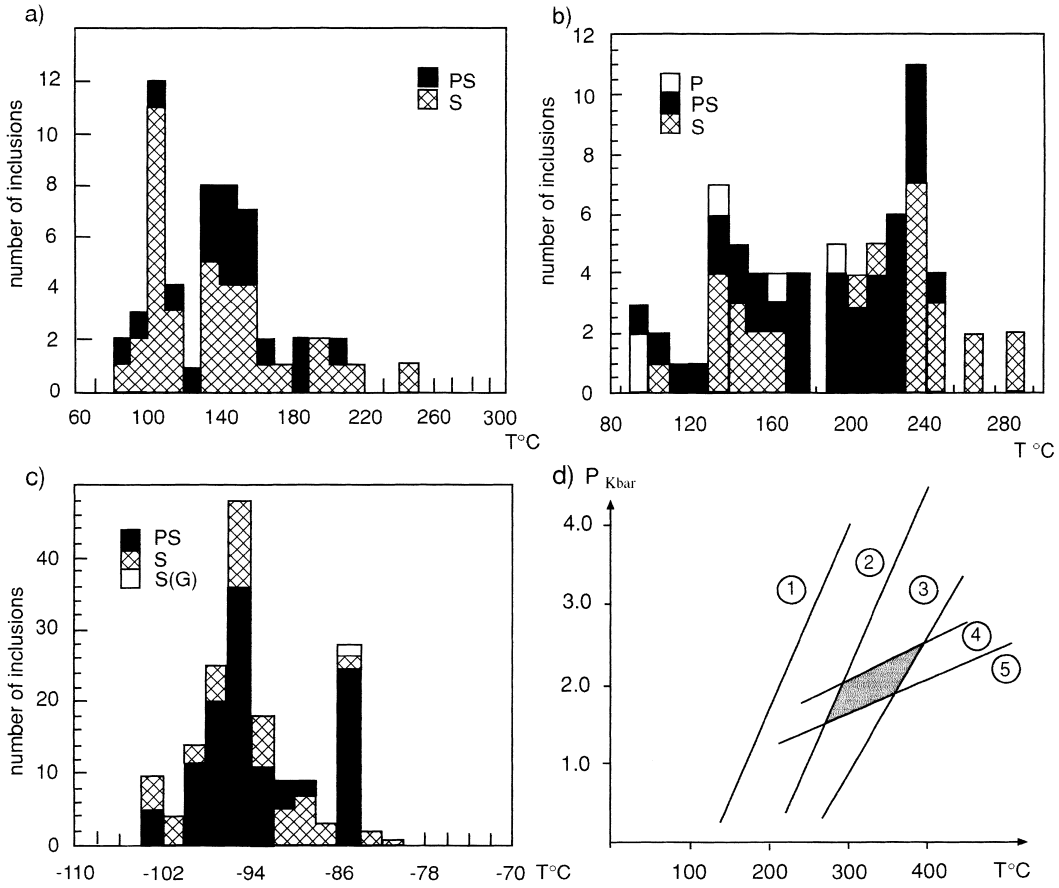

Fig. 14. Fluid inclusion data from calcite and quartz veins. (a) T_h of aqueous inclusions in fault-related calcite veins of the Bell Point and Kiln Limestones; ps and s are pseudosecondary and secondary inclusions, respectively. (b) T_h of aqueous inclusions in fold-related quartz veins (Liptrap Formation); p, ps and s are primary, pseudosecondary and secondary inclusions, respectively. (c) T_h of methane inclusions in fold-related quartz veins; ps—pseudosecondary inclusions; s and s(g)—secondary inclusions with homogenisation into the liquid and the gas phase, respectively. (d) Proposed P–T conditions of fluid inclusion trapping. 1, 2 and 3—isochores of low-salinity aqueous inclusions with T_h of 150 and 250°C, respectively (after Zhang and Frantz, 1987); 4 and 5—isochores of methane system with T_h of −100 and −90°C, respectively (after Zagoruchenko and Zhuravlev, 1970).

gations (see earlier), temperatures in the range of 160–250°C seem to be more realistic.

7. Fault exhumation history

Utilising (1) the temperature of the folding and faulting deformation inferred from the fluid inclusion data, and (2) the possible time period for deformation based on known geological contraints, an attempt has been made to determine the exhumation rate of the fault zone. The approach assumes: (1) a time lapse for deformation of ~10 Ma considering the relationship between sedimentation, deformation and plutonism within the Melbourne zone (Gray and Cull, 1992; Foster et al., 1996; Gray et al., 1997; Foster and Gray, in press; Gray and Foster, 1998); and (2) that both folding and faulting are part of the same deformation event as suggested by field relationships, despite the fact that the estimated fold and fault temperatures (290–320°C and 150–250°C, respectively) imply a time gap between folding and faulting. Time–temperature diagrams (Fig. 15) for different exhumation rates based on these assumptions were calculated using the relationship of Carslaw and Jaeger (1959, p. 388).

Only rapid exhumation rates of between 1000 and 500 m/Ma are in good agreement with the estimated temperature ranges and the assumed time lapse for deformation (Fig. 15a). Such rates of exhumation are also common in modern and ancient accretionary complexes (e.g. ~200 m/Ma calculated from Hasabe et al., 1993, figs. 4 and 5). The calculated exhumation rates and assumed geothermal gradients ($g \sim 0.03$°C/km) during fold- and fault-related deformation require that folding and faulting occurred at depths of 6–8 and 3–4 km, respectively (Fig. 15b). The derived pressure and temperature ranges are consistent with the fold- and fault-related microstructures in clastic rocks, whereas the deformation mechanisms and temperatures in limestones only represent faulting conditions. We assume that limestones were folded at a higher crustal level and later juxtaposed with the clastic sequence during faulting.

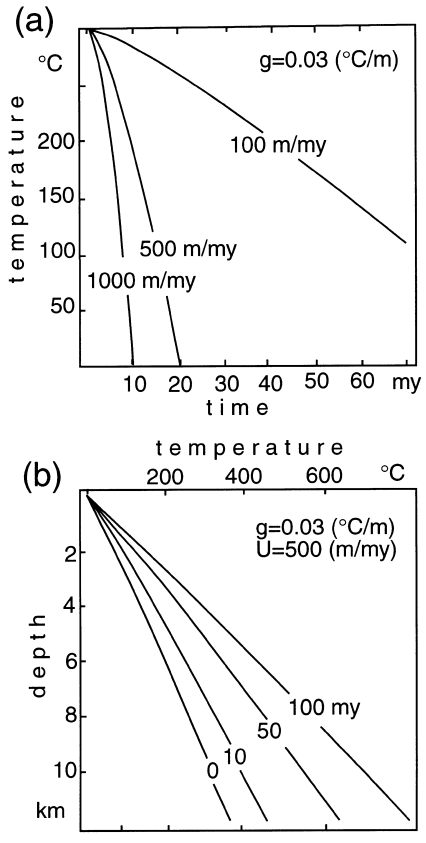

Fig. 15. Temperature–time diagram (a) and temperature–depth diagram (b) to establish exhumation rate, based upon interpretation of the fluid inclusion data and calculations from Carslaw and Jaeger (1959).

8. Discussion

The Waratah Fault Zone provides an exhumed example of a fossil fluid system where the mélange zone has very few veins. For the Waratah Fault Zone, brittle fracturing/cataclasis, pressure solution and solution transfer of material are the dominant deformation mechanisms in limestones as well as clastic sediments; however, pressure solution relicts are more abundant in limestones than in clastic sediments. Numerous microstructural examples of cross-cutting relationships between micro-veins and pressure solution seams indicate that fracturing and dissolution mechanisms occurred concurrently. Deformation twinning occurs only in calcite grains of deformed limestones. Although on the scale of the whole fault zone the deformation intensity increases toward the main fault trace, both sequences showing local variations in fracture density, fracture- and subsidiary fault orientations which are superimposed on the overall trend. As well, domains of apparent undeformed rocks have been separated by narrow zones of localised deformation. The alteration of Liptrap Formation by dehydration and dewatering during deformation (cf. Byrne, 1994), accompanied by shear-induced brecciation and subsequent solution transfer, led to the formation of an up to 100 m wide fault-mélange/gouge zone, whereas in limestones, only fault-gouge zones at centimetre scale have been developed. Such variations in deformation patterns and fault-rock alteration processes are very common in larger fault zones reflecting their spatial and temporal evolution (Chester and

Logan, 1986; Chester et al., 1993; Evans and Chester, 1995).

In contrast to fluid-assisted fault zone 'weakening' mechanisms (e.g. pressure solution/solution transfer) which are distributed over the whole fault zone, veining typifying fluid-assisted 'healing'/strain 'hardening' processes (i.e. rock-mass cementation) is largely confined to the limestone on the south side of the Waratah Fault Zone. Strain 'hardening' of the limestone sequence by cementation, and strain 'softening' of the Liptrap Formation by silica dissolution and feldspar alteration, may result from different solubilities for calcite and quartz, thereby controlling dissolution/precipitation. The solubility of calcite is determined by temperatures, pH, salts in solution and partial pressure of CO_2 (Ellis, 1959, 1963), whereas the solubility of quartz is controlled largely by temperature and pressure (e.g. Fournier and Potter, 1982; Parry, 1994). Comparing the solubility of calcite and quartz for the same fluid-composition at constant pressure, calcite solubility increases with decreasing temperature whereas quartz solubility decreases (Janssen et al., 1998). Within the fault-related temperature range (160–200°C) the solubility of calcite is significantly higher than that of quartz. However, a decrease in CO_2 by degassing may result in carbonate precipitation only. By applying these principles, the following generalisations concerning fluid–rock interaction and fluid flow in (a) the limestone sequence and (b) the Liptrap Formation can be stated:

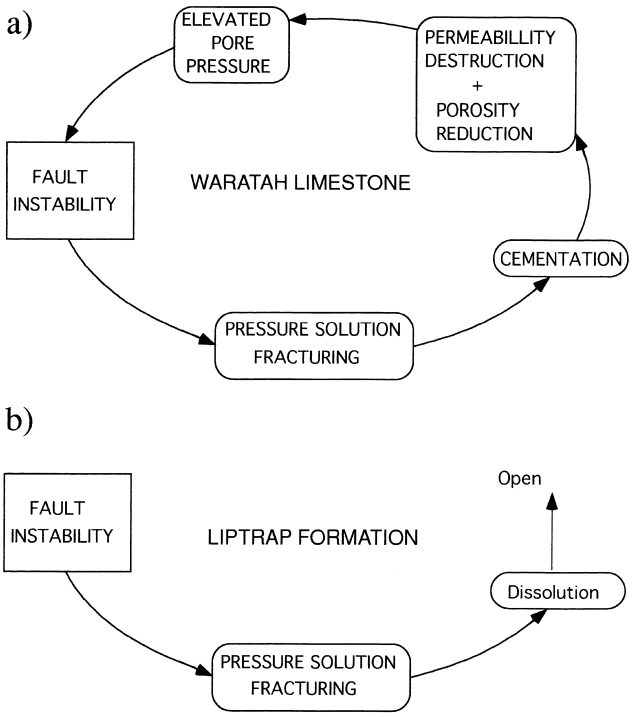

Fig. 16. Synoptic diagram of fault failure in both the limestones, and turbidites of Liptrap Formation (modified after Sibson, 1992). (a) Cyclic development of fault deformation in limestones leading to a repeated change between open and closed system with respect to fluids. (b) Lack of cementation in the fault-mélange zone prevents the creation of elevated pore pressure and as a consequence this system remains open with respect to fluids.

(a) The main concentration of calcite veins and cemented breccia zones occurs in the Bell Point Limestone between the two fault branches (major fault trace and the southern fault branch). Assuming sinistral fault movements to explain the meso-fault pattern (see Fig. 11c1), the region between the faults either forms a dilational jog (Sibson, 1986) or a zone of extremely localised deformation (Fig. 13d). Differences in fluid pressure in this zone and the surrounding rocks probably caused frictional slip and local brecciation by hydraulic implosion and subsequent fluid flow (Sibson, 1986). Fractures formed during fault displacement facilitated fluid migration and the increase of fault zone permeability (open system). With escape of CO_2, precipitation of calcite could take place. After displacement the deformation rate probably dropped below that required for fracturing and other mechanisms such as pressure solution, solution transfer and twinning became more important. The decreasing abundances of veins and breccia zones normal to the fault, indicate that the fault served as channel for calcite-bearing fluids. Results from cathodoluminesence-microscopy suggest repeated infiltration of fluids and support the assumption of the cyclic nature of fault-related deformation in the limestone sequence. We propose that the cementation of fault breccia zones leads to porosity reduction and lower permeability, connected with a relatively closed system in the limestone sequence. Hence, domains of higher pore fluid pressure could be created. Continued porosity reduction may culminate in the coalescence of elevated pore pressure domains inducing fault instability and slip (Miller et al., 1996; Janssen et al., 1998). This process caused a repeated creation and destruction of permeability within the fault-related limestones (Fig. 16a) and can be described as a combined conduit–barrier system (Caine et al., 1996).

(b) Within the tubidite sequence north of the main fault trace, deformation is concentrated in the core of the fault (fault-mélange zone), where the mélange zone rocks form due to dewatering, fracturing and brecciation, and pressure solution (see Byrne, 1994). Superimposed fracturing and faulting, as in Bell Point and Waratah Limestones, promoted fluid infiltration into the Liptrap Formation. Unsuitable conditions for precipitation of quartz in

the range of faulting temperatures however, resulted in only a few small quartz veins and a complete absence of quartz-cemented breccia. Euhedral radial quartz crystals in these veins indicate fast, wide-opening of fractures by fault slip (see fig. 7l, Gratier and Gamond, 1990). Instead of cementation, the fluids caused silica dissolution and breakdown of feldspar. We suggest that the system remained open, and that this, combined with increasing dilatation prevented the cyclic variations in fault-porosity and permeability, that are observed in the limestones (Fig. 16b). With regard to fault zone architecture and permeability structure, the mélange zone within the Liptrap Formation is mostly characterised as a localised conduit (Caine et al., 1996).

Subvertical, strike-slip fault zones, such as the Waratah Fault Zone, can occur within the frontal parts of accretionary wedges (e.g. Sample et al., 1993, fig. 1). The nature and extent of cataclasis and veining, as well as the inferred relatively shallow depth of faulting (>5 km) for the Waratah Fault Zone, are atypical for most faults within the turbidite-dominated western Lachlan Fold belt, where faulting is considered to have initiated at, and propagated from, depths of between 15 and 20 km (Cox et al., 1991; Gray et al., 1991; Cox, 1995; Gray, 1995; Gray and Foster, 1998). These deeper-level faults within the turbidite sequences have strain-softened basal zones dominated by mica growth during continued foliation development by 'transposition cycling' in a thrusting-related shear regime (cf. Gray, 1995; Gray and Foster, 1998).

In contrast, the Waratah Fault Zone has clearly developed in the shallower parts of the migrating and structurally thickening, sedimentary wedge. Scaly-matrix mélange and mud diapirism as dykes and meshwork veinlets in the fault-mélange zone (Fig. 3) are typical of fault zones in accretionary complexes (e.g. Moore, 1978). Mélange zones have been shown to be regions of high fluid flow (e.g. Vrolijk, 1987; Vrolijk et al., 1988) and most ancient mélange zones contain meshwork vein systems (e.g. Cloos, 1989, fig. 3), which are considered to represent former hydrofractures distributed parallel to the scaly fabric of the 'fault zone' (see Moore, 1989, fig. 9). In modern accretionary complexes, the major décollement at the base of the prism and subsidiary faults have been shown to be important fluid conduits (Cloos, 1984; Le Pichon et al., 1990; Sample et al., 1993; Moore et al., 1995; Screaton et al., 1997). They coincide with zones of overpressuring (Moore et al., 1995; Fisher et al., 1996) and are marked by fluids of different chemistry and isotopic composition relative to the surrounding sediment (Ritger et al., 1987; Gieskes et al., 1990; Sample et al., 1993; Sample, 1996). Fluids with elevated temperatures have been reported from modern accretionary prisms (Vrolijk et al., 1988), which may explain the anomalously high temperatures (160–200°C) relative to depth, as inferred from fluid inclusions from veins in these rocks. The geochemical and stable isotopic signatures of fault-rocks within the Waratah Fault Zone are investigated and discussed elsewhere (Janssen et al., 1998).

9. Conclusions

Fault-rock fabrics and fluid inclusion analyses have been used to determine deformation mechanisms and appropriate conditions during folding and faulting, and to evaluate the influence of varying fault-rock composition on fault strengthening and weakening processes, respectively. Although folding and faulting probably belong to the same deformation event, fold-related deformation mechanisms and corresponding temperatures were only detected in clastic sediments. Both limestones and clastic rocks are characterised by similar fault-related deformation features. Distinctions in fault-rock composition and fault geometry however, led to varying fluid-flow and different fluid–rock interactions affecting the mechanical behaviour of the fault zone. Fluid-assisted healing processes (cementation) are largely confined to the limestone sequence, where microscopic observations indicate that faulting involved repeated episodes of fault failure and fault healing. Here, the fault acts as a conduit–barrier system. In contrast, the fractured and faulted Liptrap Formation exhibits dissolution and solution transfer in the formation of a fault-mélange zone. Fault-rock healing processes (cementation) are missing. This zone remains open with respect to fluids and represents a conduit system.

Acknowledgements

The research was undertaken during a visit by CJ to Monash University under the sponsorship of a Deutscher Akademischer Austauschdienst. Support for the project was also from an ARC95 Small Grant and ARC Large Grant A39601548 awarded to DRG for work on fluid–rock interaction in fault zones. We thank Kurt Stuwe for helping calculate the exhumation rate, Michel Gero for calculating the strain axes from the fault slip data, Draga Gelt, Sylvia Zakowski, and Anna Klein for help with drafting, and Andy McCaig, Richard Norris and an anonymous reviewer for constructive reviews which significantly improved the manuscript.

Appendix A. Fluid inclusion analyses

A.1. Sampling details and analytical methods

Fluid inclusion studies were carried out on calcite and quartz veins from a horizontal profile across the Waratah Fault Zone. The samples are from different lithologies with varying deformation intensity. All calcite veins result from fault-related deformation processes, whereas quartz veins formed during both fold and faulting events.

The fluid inclusions were investigated by microthermometry using a standard Fluid Inc. heating–freezing stage. The stage was calibrated using melting temperatures of butyl-chloride (−123.1°C) and Fluid Inc. standards: Melting temperature of CO_2 (−56.6°C), eutectic temperatures of H_2O–NaCl (−21.2°C) and H_2O–KCl solutions (−10.7°C). The accuracy of temperature measurements is ±0.5°C at low temperature range (−180 ± 50°C) and ±5°C at high temperature range (100–500°C).

A.2. Results

Aqueous inclusions have only been detected in blocky calcite grains within calcite veins. The inclusions vary between 5 and 7 μm in diameter. At ambient temperature, they are usually two phase inclusions (liquid + gas) with a small gas bubble. The fluid inclusion planes mainly cut across grain boundaries forming secondary trails of fluid inclusions (Roedder, 1984). Rare fluid inclusion planes are terminated at grain boundaries, and are probably of pseudosecondary origin (Roedder, 1984). In a few cases, during heating–freezing experiments, the final melting temperature (T_{mf}) of ice was measured in the range between −5.0 and −2.0°C indicating a salinity of brine solution from 8 to 3 eq. wt.% NaCl (Potter et al., 1978). The data on the homogenisation temperature (T_h) of aqueous inclusions (liquid + gas → liquid) are shown in Fig. 14(a). It is evident that pseudosecondary and secondary inclusions have the same characteristics. The inclusions usually homogenised from 100 to 160°C with a smaller subset of inclusions between 180 and 240°C.

Fluid inclusions in quartz veins were only detected in fold-related veins. Here, two-fluid inclusion systems (aqueous and gaseous inclusions) with different compositions were found and analysed. Microthermometric investigation showed that they were brine and methane inclusions, respectively. Fluid inclusions are distributed in fissure quartz and represented by fluid inclusion planes inside the fibre quartz. It is likely that fluid inclusion planes are composed of pseudosecondary inclusions (Mullis, 1987). Often several planes of inclusions cut across quartz fibres forming secondary trails. Randomly distributed aqueous inclusions were found in a few quartz crystals. These inclusions are probably primary (Roedder, 1984). In a few cases planes of aqueous and gaseous inclusions occur along the same trail, but more often aqueous and gaseous inclusions form separate trails having similar direction and dip angle.

All aqueous inclusions contain liquid and gas phases. The inclusion size is up to 10 μm. Freezing melting of ice occurred at T_{mf} from −6.0 to −2.0°C reflecting salinities in the range between 9 and 2 eq. wt% NaCl (Potter et al., 1978). In one inclusion initial melting of ice was marked at T_{mf} of −9.0°C, which points to a KCl solution (Borisenko, 1982). The homogenisation temperatures of the aqueous inclusions varied between 130 and 250°C (Fig. 14b).

Gaseous inclusions are single-phase inclusions and in most cases they are bigger than aqueous inclusions. Freezing of the gaseous inclusions showed heterogeneity at temperatures below −100°C. Homogenisation temperatures of gaseous inclusions varied between −104 and −82°C (Fig. 15c). Several inclusions show critical behaviour at temperatures from about −86 to −82°C and one inclusion has homogenised into the gas phase at T_h of 85°C. Such behaviour is typical for methane inclusions (Mullis, 1987). It is worthwile to note that the T_h of aqueous inclusions coexisting with methane inclusions is from 180 to 250°C.

References

Alderton, D.H.M., Bevins, R.E., 1996. *P–T* conditions in the South Wales Coalfield: evidence from coexisting hydrocarbon and aqueous fluid inclusions. Journal of the Geological Society of London 153, 265–275.

Allimendinger, R.W., 1989. Notes on Fault Slip Analysis. Short Course on the Quantitative Interpretation of Joints and Faults. Department of Geological Sciences, Cornell University, Ithaca, New York.

Blanpied, M.L., Lockner, D.A., Byerlee, J.D., 1992. An earthquake mechanism based on rapid sealing of faults. Nature 358, 574–576.

Borisenko, A.S., 1982. Analysis of the salt composition of gas–liquid inclusions in minerals with the help of criometrical method. Application of Thermobarogeochemical Methods for Prospecting and Study of Ore Deposits. Nedra, Moscow, pp. 37–46 (in Russian).

Bucher, M., Foster, D.A., Gray, D.R., 1996. Timing of cleavage development in the western Lachlan Fold Belt: new constraints from $^{40}Ar/^{39}Ar$ thermochronology. Geological Society of Australia Abstracts 41, 66.

Burkhard, M., 1993. Calcite-twins, their geometry, appearance and significance as stress–strain markers and indicators of tectonic regime: a review. Journal of Structural Geology 15, 351–368.

Byrne, T., 1994. Sediment deformation, dewatering and diagenesis: illustrations from selected mélange zones. In: Maltman, A. (Ed.), Geological Deformation of Sediments. Chapman & Hall, London, pp. 239–260.

Caine, J.S., Evans, J.P., Forster, C.B., 1996. Fault zone architecture and permeability structure. Geology 24, 1025–1028.

Carslaw, H.S., Jaeger, C.J., 1959. Conduction of Heat in Solids, 2nd ed. Clarendon Press, Oxford.

Cas, R.A.F., VandenBerg, A.H.M., 1988. Ordovician. In: Douglas, J.G., Ferguson, J.A. (Eds.), Geology of Victoria. Geological Society of Australia Victorian Division, Melbourne, pp. 63–102.

Chester, F.M., 1994. Rheologic model of crustal faults: influence of fluids on strength and stability. The Mechanical Involvement of Fluids in Faulting. US Geological Survey Open-file Report 94-228 (Proceedings of Workshop LXIII), pp. 487–501.

Chester, F.M., Logan, J.M., 1986. Implication for mechanical properties of brittle faults from observations of Punchbowl fault zone, California. Pure and Applied Geophysics 124, 79–106.

Chester, F.M., Logan, J.M., 1987. Composite planar fabric of gouge from the Punchbowl Fault, California. Journal of Structural Geology 9, 621–634.

Chester, F.M., Evans, J.P., Biegel, R.L., 1993. Internal structure and weakening mechanisms of faults of the San Andreas Fault system. Journal of Geophysical Research 98, 771–786.

Cloos, M., 1984. Landward-dipping reflectors in accretionary wedges: active dewatering conduits? Geology 12, 519–522.

Cox, S.F., 1995. Faulting processes at high fluid pressures: An example of fault valve behaviour from the Wattle Gully Fault, Victoria, Australia. Journal of Geophysical Research 100, 12,841–12,859.

Cox, S.F., Etheridge, M.A., 1989. Coupled grain-scale dilatancy and mass transfer during deformation at high fluid pressures: examples from Mount Lyell, Tasmania. Journal of Structural Geology 11, 147–162.

Cox, S.F., Etheridge, M.A., Cas, R.A.F., Clifford, B.A., 1991. Deformational style of the Castlemaine area, Bendigo–Ballarat Zone: implications for evolution of crustal structure in central Victoria. Australian Journal of Earth Sciences 38, 151–170.

Elliott, C.G., Woodward, N.B., Gray, D.R., 1993. Complex regional fault history in the Badger Head region, northern Tasmania. Australian Journal of Earth Sciences 40, 155–168.

Ellis, A.J., 1959. The solubility of calcite in carbon dioxide solutions. American Journal of Science 257, 354–365.

Ellis, A.J., 1963. The solubility of calcite in sodium chloride solutions at high temperatures. American Journal of Science 261, 259–267.

Evans, J.P., Chester, F.M., 1995. Fluid–rock interaction in faults of the San Andreas system: inferences from San Gabriel fault rock geochemistry and microstructures. Journal of Geophysical Research 100, 13,007–13,020.

Fisher, A.T., Zwart, G. et al., 1996. Relation between permeability and effective stress along a plate-boundary fault, Barbados accretionary complex. Geology 24, 307–310.

Foster, D.A., Gray, D.R., in press. Chronology of deformation in the turbidite-dominated Lachlan Orogen: implications for the tectonic evolution of eastern Australia and Gondwana. Tectonics.

Foster, D.A., Gray, D.R., Offler, R., 1996. The western subprovince of the Lachlan Fold Belt, Victoria: structural style, geochronology, metamorphism and tectonics. Specialist Group in Geochemistry, Mineralogy, and Petrology Field Guide No. 1, Geological Society of Australia, Sydney.

Foster, D.A., Gray, D.R., Kwak, T.A.P., Bucher, M., 1998. Chronologic and orogenic framework of turbidite hosted gold deposits in the western Lachlan Fold Belt, Victoria. Ore Geology Reviews 13, 229–250.

Fournier, R.O., Potter, R.W., II, 1982. An equation correlating the solubility of quartz in water from 25°C to 900°C at pressures up to 10,000 bars. Geochimica et Cosmochimica Acta 46, 1969–1973.

Garrat, M.J., 1983. Silurian to Early Devonian facies and biofacies patterns for the Melbourne Trough, central Victoria. Journal of the Geological Society of Australia 30, 121–147.

Gieskes, J.M., Vrolijk, P., Blanc, G., 1990. Hydrogeochemistry of the northern Barbados accretionary complex transect: ocean drilling project Leg 110. Journal of Geophysical Research 95, 8809–8818.

Gratier, J.P., Gamond, J.F., 1990. Transition between seismic and aseismic deformation in the upper crust. In: Knipe, R.J., Rutter, E.H. (Eds.), Deformation Mechanisms, Rheology and Tectonics. Geological Society of London Special Publication 54, 461–473.

Gray, C.M., 1990. A strontium isotopic traverse across the granitic rocks of southeastern Australia: petrogenetic and tectonic implications. Australian Journal of Earth Sciences 37, 331–349.

Gray, D.R., 1988. Structure and tectonics. In: Douglas, J.G., Ferguson, J.A. (Eds.), Geology of Victoria. Geological Society of Australia Victorian Division, Melbourne, pp. 1–36.

Gray, D.R., 1995. Thrust kinematics and transposition fabrics from a basal detachment zone, eastern Australia. Journal of Structural Geology 17, 1637–1654.

Gray, D.R., 1997. Tectonics of the southeastern Australian Lachlan Fold Belt: structural and thermal aspects. In: Burg, J.P., Ford, M. (Eds.), Orogeny through Time. Geological Society of London Special Publication 121, pp. 149–177.

Gray, D.R., Cull, J.P., 1992. Thermal regimes, anatexis, and orogenesis; relations in the western Lachlan Fold Belt, southeastern Australia. Tectonophysics 214, 441–461.

Gray, D.R., Foster, D.A., 1997. Orogenic concepts—application and definition: Lachlan Fold Belt, eastern Australia. American Journal of Science 297, 859–891.

Gray, D.R., Foster, D.A., 1998 Character and kinematics of faults within a structurally thickened subduction–accretion system, Lachlan Orogen: implications for the tectonic evolution of eastern Australia. Journal of Structural Geology 20, 1691–1720.

Gray, D.R., Mortimer, L., 1996. Implications of overprinting deformations and fold interference patterns in the Melbourne Zone, Lachlan Fold Belt. Australian Journal of Earth Sciences 43, 103–114.

Gray, D.R., Willman, C.E., 1991a. Thrust-related strain gradients and thrusting mechanisms in a chevron-folded sequence, south-eastern Australia. Journal of Structural Geology 13, 691–710.

Gray, D.R., Willman, C.E., 1991b. Deformation in the Ballarat Slate Belt, Central Victoria and implications for the crustal structure across SE Australia. Australian Journal of Earth Sciences 38, 171–201.

Gray, D.R., Wilson, C.J.L., Barton, T.J., 1991. Intracrustal detachments and implications for crustal evolution within the Lachlan Fold Belt, southeastern Australia. Geology 19, 574–577.

Gray, D.R., Foster, D.A., Bucher, M., 1997. Recognition and definition of orogenic events in the Lachlan Fold Belt. Australian Journal of Earth Sciences 44, 489–501.

Hadizadeh, J., 1994. Interaction of cataclasis and pressure solution in a low-temperature carbonate shear zone. Pure and Applied Geophysics 134, 255–280.

Hasabe, N., Tagami, T., Nishimura, S., 1993. Evolution of the Shimanto accretionary complex: a fission track thermochronologic study. In: Underwood, M.B. (Ed.), Thermal Evolution of the Tertiary Shimanto Belt, Southwest Japan: an example of ridge–trench interaction. Geological Society of America Special Paper 273, 121–136.

Hickmann, S.H., 1990. Stress in the lithosphere and the strength of active faults. Reviews of Geophysics 29, 759–776.

Hirth, G., Tullis, J., 1989. The effects of pressure and porosity on the micromechanics of the brittle–ductile transition in quartzite. Journal of Geophysical Research 94, 17,825–17,838.

Janssen, C., Michel, G.W., Bau, M., Lüders, V., Mühle, K., 1997. The North Anatolian Fault Zone and the role of fluids in seismogenic deformation. Journal of Geology 105, 387–403.

Janssen, C., Laube, N., Bau, M., Gray, D.R., 1998. Fluid regime in faulting deformation of the Waratah Fault zone, Australia, as

inferred from major and minor element analyses and stable isotopic signatures. Tectonophysics, 294, 109–130.
Knipe, R.J., Lloyd, G.E., 1994. Microstructural analysis of faulting in quartzite, Assynt, NW Scotland: implications for fault zone evolution. Pure and Applied Geophysics 143, 229–254.
Lennox, P.G., Golding, S.D., 1989. Quartz veining in simply folded arenites, Cape Liptrap, Southeast Victoria, Australia. Australian Journal of Earth Sciences 36, 243–261.
Le Pichon, X., Henry, P., Lallement, S., 1990. Water flow in the Barbados accretionary complex. Journal of Geophysical Research 95, 8945–8967.
Lindner, A.W., 1953. The geology of the coastline of Waratah Bay between Walkerville and Cape Liptrap. Proceedings of the Royal Society of Victoria 64, 77–92.
Logan, J.M., Dengo, C., Higgs, N., Wang, Z.Z., 1992. Fabrics of experimental fault zones: Their development and relationship to mechanical behaviour. In: Wong, B., Evans, T.F. (Eds.), Fault Mechanics and Transport Properties in Rocks. Academic Press, London, pp. 33–68.
Marrett, R., Alimendinger, R.W., 1990. Kinematic analysis of fault slip data. Journal of Structural Geology 12, 973–986.
Michel, G.W. (1994) Neo-kinematics along the North-Anatolien Fault (Turkey). Tübingen Geowischenschafte Arbeit, Reihe A 16.
Michel, G.W., Waldhör, M., Neugebauer, J., Appel, E., 1995. Sequential rotation of stretching axes, and block rotations: A structural and palaeomagnetic study along the North-Anatolien Fault. Tectonophysics 243, 97–118.
Miller, S.A., Nur, A., Olggaard, D.L., 1996. Earthquakes as a coupled shear stress–high pore pressure dynamical system. Geophysical Research Letters 23, 197–200.
Moore, J.C., 1978. Orientation of underthrusting during latest Cretaceous and earliest Tertiary time, Kodiak Islands, Alaska. Geology 6, 209–213.
Moore, J.C., 1989. Tectonics and hydrogeology of accretionary prisms: role of the décollement zone. Journal of Structural Geology 11, 95–106.
Moore, J.C. et al, 1995. Abnormal fluid pressures and fault-zone dilation in the Barbados accretionary prism: evidence from logging while drilling. Geology 23, 605–608.
Mullis, J., 1987. Fluid inclusion studies during very low-grade metamorphism. In: Frey, M. (Ed.), Low Temperature Metamorphism. Blackie, London, pp. 162–199.
Murphy, N.C., Gray, D.R., 1992. East-directed overthrusting in the Melbourne Zone, Lachlan Fold Belt. Australian Journal of Earth Sciences 39, 37–53.
Nas, D., 1988. Early Devonian turbidite sedimentation along the eastern margin of the Melbourne Terrane. Unpublished MSc thesis, Monash University.
Newman, J., Mitra, G., 1993. Lateral variations in mylonite zone thickness as influenced by fluid–rock interactions, Linville Falls fault, North Carolina. Journal of Structural Geology 15, 849–863.
Newman, J., Mitra, G., 1994. Fluid-influenced deformation and recrystallization of dolomite at low temperatures along a natural fault zone, Mountain City window, Tennessee. Geological Society of America Bulletin 106, 1267–1280.
Nicholls, I.A., 1965. Studies on the mineralogy, petrology and chemistry of the greenstones of the Heathcote District, Victoria. Unpublished MSc thesis, University of Melbourne.
O'Connor, B., 1978. The sedimentary and tectonic structures of the Lower Devonian Liptrap Formation, Victoria. Unpublished PhD thesis, University of Melbourne.
Offler, R., McKnight, S., Morand, V.J., 1998. Tectono-thermal history of the western Lachlan Fold Belt, Australia—insights from white mica studies. Journal of Metamorphic Geology 16, 531–540.
Parry, W.T., 1994. Fault fluid composition from fluid inclusion observations. The Mechanical Involvement of Fluids in Faulting, US Geological Survey Open-file Report 94-228 (Proceedings of Workshop LXIII), pp. 334–348.
Paterson, M.S., 1978. Experimental Rock Deformation—the brittle field. Springer, Heidelberg.
Potter, R.W., II, Clynne, M.A., Brown, D.L., 1978. Freezing point depression of aqueous sodium chloride solutions. Economic Geology 73, 284–285.
Powell, C.McA., Baillie, P.W., 1992. Tectonic affinity of the Mathinna Group in the Lachlan Fold Belt. Tectonophysics 214, 193–209.
Ramsay, J.G., 1980. The crack–seal mechanism of rock deformation. Nature 284, 135–139.
Ramsay, W.R.H., VandenBerg, A.H.M., 1986. Metallogeny and tectonic development of the Tasman Orogen system in Victoria. Ore Geology Reviews 1, 149–160.
Reches, Z., 1978. Analysis of faulting in three-dimensional strain field. Tectonophysics 47, 109–129.
Reches, Z., 1983. Faulting of rocks in three-dimensional strain fields II. Theoretical analysis. Tectonophysics 95, 133–156.
Rice, J.R., 1992. Fault stress states, pore pressure distributions, and the weakness of the San Andreas fault. In: Wong, B., Evans, T.F. (Eds.), Fault Mechanics and Transport Properties in Rocks. Academic Press, London, pp. 475–503.
Richards, J.R., Singleton, O.P., 1981. Palaeozoic Victoria, Australia: igneous rocks, ages and their interpretation. Journal of the Geological Society of Australia 28, 395–421.
Ritger, S., Carson, B., Suess, E., 1987. Methane-derived authigenic carbonates formed by subduction-induced pore-water expulsion along the Oregon/Washington margin. Geological Society of America Bulletin 98, 147–156.
Roedder, W., 1984. Fluid inclusions. Reviews in Mineralogy No. 12. Mineralogical Society of America, Washington DC.
Sample, J.C., 1996. Isotopic evidence from authigenic carbonates for rapid upward fluid flow in accretionary wedges. Geology 24, 897–900.
Sample, J.C., Reid, M.R., Tobin, H.J., Moore, J.C., 1993. Carbonate cements indicate channeled fluid flow along a zone of vertical faults at the deformation front of the Cascadia accretionary wedge (northwest U.S. coast). Geology 21, 507–510.
Scholz, C.H., 1989. Mechanics of faulting. Annual Reviews of Earth Planetary Sciences 17, 309–334.
Scholz, C.H., Dawers, P., Anders, M.H., 1994. The permeability of faults. The Mechanical Involvement of Fluids in Faulting. US Geological Survey Open-file Report 94-228 (Proceedings of Workshop LXIII), pp. 247–252.
Screaton, E.J., Fisher, A.T., Carson, B., Becker, K., 1997. Barbados Ridge hydrologic tests: implications for fluid migration along an active décollement. Geology 25, 239–242.
Sibson, R.H., 1986. Brecciation in fault zones: inferences from earthquake rupturing. Pure and Applied Geophysics 124, 159–173.
Sibson, R.H., 1989. Earthquake faulting as a structural process. Journal of Structural Geology 11, 1–14.
Sibson, R.H. (1990) Conditions for fault-valve behaviour. In: Knipe, R.J., Rutter, E.H. (Eds.), Deformation Mechanisms, Rheology and Tectonics. Geological Society of London Special Publication No. 54, pp. 15–28.
Sibson, R.H., 1992. Implications of fault-valve behaviour for rupture nucleation and recurrence. Tectonophysics 192, 283–293.
Soesoo, A., Bons, P.D., Gray, D.R., Foster, D.A., 1997. Double divergent subduction: tectonic and geologic consequences. Geology 25, 755–758.
Spaggiari, C.V., Gray, D.R., Foster, D.A., 1998. Tectonic significance of oceanic crustal slices and intermediate *P* metamorphism in the western Lachlan Fold Belt, Victoria. Geological Society of Australia Abstracts 49, 420.
Talent, J.A., 1965. The stratigraphic and disatrophic evolution of central and eastern Victoria in middle Paleozoic. Proceedings of the Royal Society of Victoria 79, 179–195.

VandenBerg, A.H.M., 1975. Definitions and descriptions of Middle Ordovician to Middle Devonian rock units in the Warburton District, East Central Gippsland. Report of the Geological Survey of Victoria 1975/76.

VandenBerg, A.H.M., 1988. Silurian–Middle Devonian. In: Douglas, J.G., Ferguson, J.A. (Eds.), Geology of Victoria. Geological Society of Australia Victorian Division, Melbourne, pp. 103–146.

VandenBerg, A.H.M., Wilkinson, E., 1982. Victoria. In: Cooper, R.A., Grindley, G.W. (Eds.), Late Proterozoic to Devonian Sequences of Southeastern Australia, Antarctica and New Zealand and their Correlation. Geological Society of Australia Special Publication No. 9, pp. 36–47.

Vrolijk, P., 1987. Tectonically driven fluid flow in the Kodiak accretionary complex, Alaska. Geology 15, 466–469.

Vrolijk, P., Myers, G., Moore, J.C., 1988. Warm fluid migration along tectonic melanages in the Kodiak Accretionary Complex, Alaska. Journal of Geophysical Research 93, 10,313–10,324.

Woodward, N.B., Gray, D.R., Elliott, C.G., 1993. Repeated thrusting and allochoneity of Precambrian basement, northern Tasmania. Australian Journal of Earth Sciences 40, 297–311.

Zagoruchenko, V.A., Zhuravlev, A.M., 1970. Thermophysical Properties of Gaseous and Liquid Methane. Israel Progress Science Translations, Jerusalem.

Zhang, Y.-G., Frantz, J.D., 1987. Determination of the homogenization temperatures and densities of supercritical fluids in the system $NaCl–KCl–CaCl_2–H_2O$ using synthetic fluid inclusions. Chemical Geology 64, 335–350.